A numerical study of the February 15, 1941 storm in the Tagus estuary

André B. Fortunato[1]; Paula Freire[2]; Xavier Bertin[3]; Marta Rodrigues[4]; Juan Ferreira[5]; Margarida L.R. Liberato[6]

Full text available at: http://www.sciencedirect.com/science/article/pii/S027843431630512X

Please cite as: Fortunato, A.B., P. Freire, X. Bertin, M Rodrigues, J. Ferreira, M.L.R. Liberato (2017). A numerical study of the February 15, 1941 storm in the Tagus estuary, *Continental Shelf Research*, 144: 50-64, DOI: 10.1016/j.csr.2017.06.023

Abstract

On February 15, 1941, a storm caused one of the major natural disasters in the Iberian Peninsula in the past century. The storm made landfall in the north of Portugal, leading to a large surge in the Tagus estuary. Adverse meteorological conditions combined with a high spring tide led to extensive flooding of dry land, causing severe damage and casualties. A suite of regional and local scale models is developed to analyze the event and the relative contributions of the different forcing agents to the extreme water levels. Quantitative and qualitative validations show that the models adequately reproduce this type of events. The models are then used to assess the inundation in the upstream reaches of the estuary where extensive agricultural lands are protected by dikes. Results show that over 25 km^2 could be inundated today, a value that would increase threefold for a sea level rise of 0.5 m. Then, the relative importance of the different forcing mechanisms on the extreme water levels is investigated through numerical experiments. It is shown that the regional surge and the setup induced by swell are the two main drivers of the inundation. In particular, the modulation of the wave setup by tides induces a semi-diurnal signal which is amplified by resonance inside the estuary.

Highlights:

- Hindcast of the most severe storm of the 20th century in the Iberian Peninsula
- Physical drivers for flooding are identified
- Regional surge and swell-driven setup are the main causes of storm surge
- Wave setup is modulated by tides and amplified by resonance
- Extensive agricultural lands can be submerged

Keywords: tide-surge interaction; numerical modeling; SCHISM; flooding; 2010 Xynthia storm; Portugal.

1 National Laboratory for Civil Engineering, Av. do Brasil 101, 1700-066 Lisbon, Portugal, afortunato@lnec.pt.
2 National Laboratory for Civil Engineering, Av. do Brasil 101, 1700-066 Lisbon, Portugal, pfreire@lnec.pt.
3 UMR 7266 LIENSs, CNRS - Université de La Rochelle, 2 rue Olympe de Gouges, 17000 La Rochelle Cedex, France, xbertin@univ-lr.fr
4 National Laboratory for Civil Engineering, Av. do Brasil 101, 1700-066 Lisbon, Portugal, mfrodrigues@lnec.pt.
5 Escola de Ciências e Tecnologia, Universidade de Trás-os-Montes e Alto Douro (UTAD), Vila Real, Portugal, juan.g.ferreira@gmail.com
6 Escola de Ciências e Tecnologia, Universidade de Trás-os-Montes e Alto Douro (UTAD), Vila Real, Portugal, and Instituto Dom Luiz, Faculdade de Ciências, Universidade de Lisboa, Lisboa, Portugal, mlr@utad.pt

1. INTRODUCTION

Coastal inundations, caused by a combination of tides and storm surges, constitute major natural catastrophes. Recent examples include the devastation of parts of New Orleans by hurricane Katrina in 2005, the inundation of the south-western French coast by the Xynthia storm in 2010 and the ravage of the Philippines by typhoon Haiyan in 2013. Climate change is aggravating this hazard through sea level rise and, in some regions, increased storminess (e.g., Lowe and Gregory, 2005). Simultaneously, the growing settlement of populations in coastal regions increases their vulnerability. There is therefore a strong societal and economic motivation to address this problem.

Several avenues have been explored to mitigate this problem. Inundation maps have been developed to determine the hazard and assist in planning (e.g., Dietrich et al., 2010; Fortunato et al., 2013; Bertin et al., 2014; Le Roy et al., 2015; Tomás et al., 2015; Bilskie et al., 2016; Perini et al., 2016). Forecast systems allow the anticipation of extreme events and support first responses (e.g., Zampato et al., 2016; Fortunato et al., 2017). Appropriate solutions are designed to reduce and mitigate the effects of inundations (e.g., Zorndt et al., 2014). On a more fundamental level, a better understanding of the relative importance of the physical drivers responsible for extreme water levels is required (e.g., Melet et al., 2016). This understanding can help us to anticipate worst case scenarios, select the most appropriate tools to study the problem and design better solutions.

In this scope, much can be learned from the study of past extreme events. The analysis of their consequences indicates where emergency response is most necessary. The assessment of the effectiveness of the response can help us improve the emergency procedures. Inundation maps for past events can be produced to determine the hazard or to test the effectiveness of different solutions. These events can also help define worst case scenarios, by varying the forcing conditions within reasonable limits (Goutx et al., 2014, Lin and Emmanuel, 2016). Finally they provide severe but realistic settings to analyze the importance of the different physical drivers.

In areas where catastrophic events are rare, and thus both the authorities and the general public are less aware of their potential impacts, the search for the most extreme events can lead to a time when little quantitative data were available, and newspapers were the major source of information. In these cases, models are particularly useful, filling in the information gap (e.g. Breilh et al., 2014). Fortunately, the recent availability of long atmospheric reanalyses, such as 20CRv2 (Compo et al., 2011), opens the route to simulate and analyze these more ancient events (e.g. Stucki et al. 2015).

The Tagus estuary (in the Portuguese nearshore close to Lisbon) is an example of an area that has not suffered any major catastrophic flood in recent years. This estuary is vulnerable to inundations, due to a combination of high urbanization of its margins (Tavares et al., 2015) and extensive low-lying marginal areas. Over the past decades, a few events have inundated the margins and caused moderate damage, but no casualties were reported (Freire et al., 2016). Among them, the 2010 Xynthia storm caused the submersion of some urban areas and the overtopping of dikes. However, these recent storms were relatively mild compared to the one that hit the Iberian Peninsula on February 15, 1941. According to Muir-Wood (2011), this was one of the five most severe wind storms across Europe in the 20th century, from an impact

perspective. This storm caused widespread destruction and casualties along the Portuguese coast (Freitas and Dias, 2013), including at least 130 casualties (Muir-Wood, 2011). This author estimated that, if that storm occurred nowadays, the damage would amount to 5 billion euros in Portugal alone. Because this storm occurred at a time when systematic data gathering was still scarce, testimonies from newspapers represent the major source of information.

This paper aims at learning from the February 15, 1941 storm. The first goal is to provide new quantitative atmospheric and oceanographic elements about this important event. The second goal is to evaluate the consequences of an extreme storm in the Tagus estuary by determining the inundation extent that a similar storm would cause today, focusing on the extensive low-lying terrains of the left margin of the estuary. Simulations are therefore performed for the atmospheric and ocean conditions of 1941, but for the present bathymetry and mean sea level. The ultimate goal of this paper is to determine the relative importance of the different physical processes on the extreme water levels in the Tagus estuary.

The study is conducted by simulating atmospheric, ocean and estuarine dynamics. The atmospheric model WRF-ARW (Skamarock et al., 2008) is used first over the North Atlantic to downscale results from the 20CRv2 reanalysis. The same atmospheric model is used with a finer resolution to provide the forcing for the estuarine wave and circulation model. Results are then used to force regional wave (WAVEWATCH III ® - WW3, Tolman, 2009) and tide/surge (Semi-implicit Cross-scale Hydroscience Integrated System Model - SCHISM, Zhang et al., 2016) models to provide the boundary conditions for the estuarine model. Finally, extreme water levels in the Tagus estuary are obtained with a coupling of SCHISM with a spectral short-wave model (Wind Wave Model – WWM). The coupled circulation/wave model is denoted SCHISM-WWM (Roland et al., 2012). All relevant physical drivers are considered in the simulations: tides, waves, wind, atmospheric pressure and river flow. Numerical experiments are carried out to determine the inundation extent and the relative importance of the different physical drivers.

This paper is organized in five sections besides this introduction. Section 2 describes the study area and the storms that are studied herein: the 1941 storm and the 2010 Xynthia storm, which is used for model validation. Section 3 presents the data available for model calibration and validation. The models and their application are presented in Section 4. Section 5 presents and discusses the results. The final section summarizes the main conclusions.

2. STUDY AREA

2.1. The Tagus estuary and its margins

Located in the western Portuguese coast (Figure 1), the Tagus estuary is a mesotidal, coastal plain estuary (Figure 2a). It has a surface area of about 320 km^2, with a deep, long and narrow tidal inlet connecting the Atlantic Ocean to a shallow, tide-dominated basin. This basin has extensive tidal flats and marshes that cover about 40% of the inner estuary. About 40 km upstream, the estuary markedly narrows at the bay head. In this area, the estuary is bordered by low elevation terrains extensively used for agriculture and generally protected by dikes (Figure 2b). The estuarine bottom is mainly composed of silt and sand, of both fluvial and local origins; marine sands are confined to the mouth and inlet channel (Freire et al., 2007).

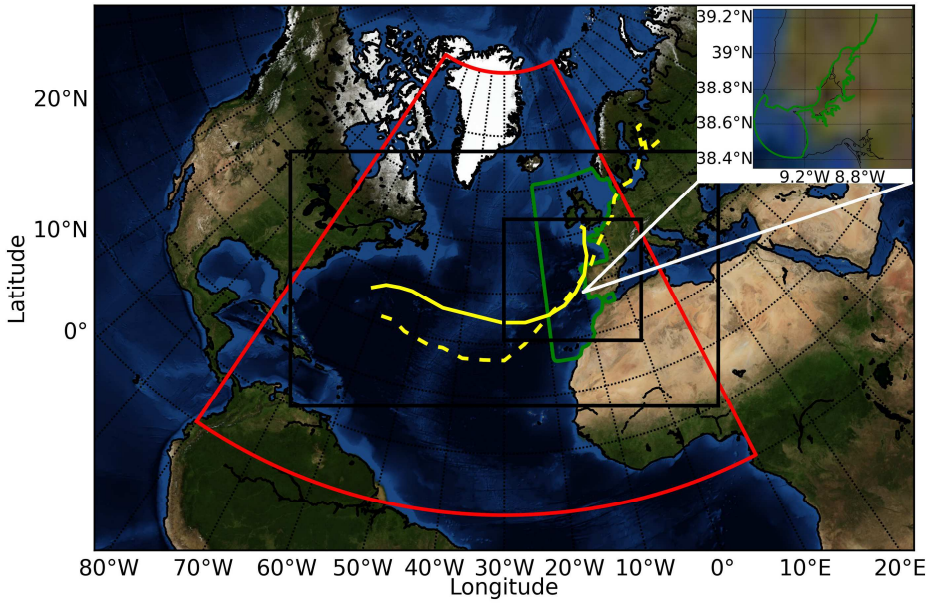

Figure 1. General location: North Atlantic, showing the boundaries of the atmospheric model regional and local grids in black, of the wave model grid in red, of the tide and tide/surge model grid in green. The yellow lines represent the trajectory of the center of the 1941 (solid line) and 2010 (dashed line - Xynthia) storms. The trajectories were determined based on the atmospheric model results described below. The inset shows the boundaries of the Tagus estuary grid.

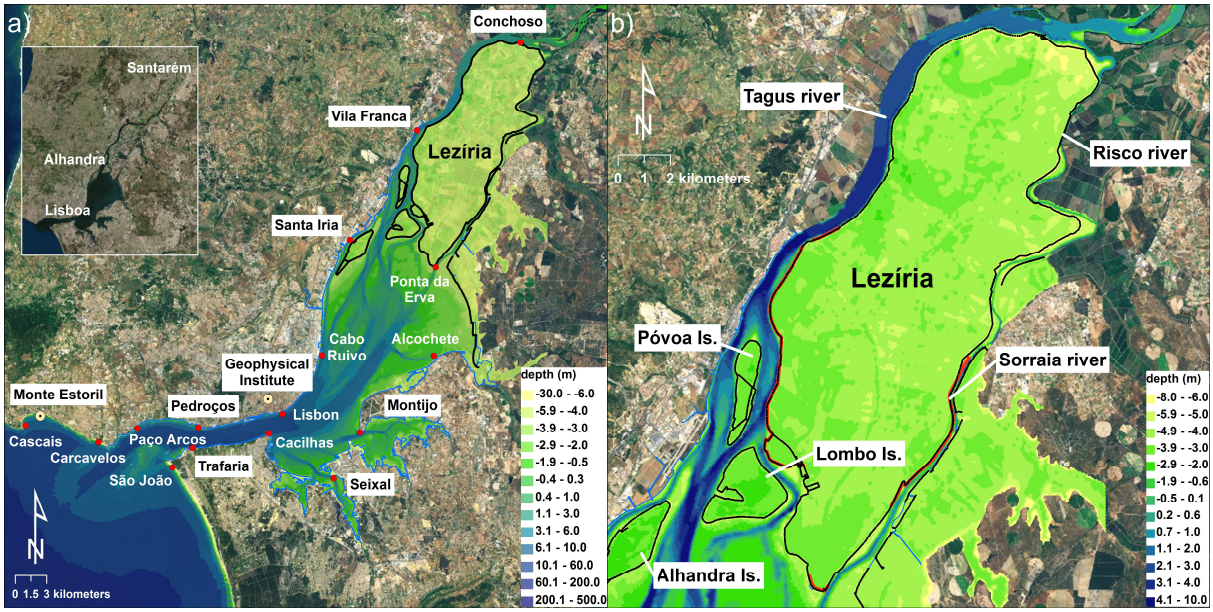

Figure 2. Tagus estuary bathymetry relative to chart datum (interpolated onto the model grid) and place names: a) global view; b) detail of the inundation-prone areas of the upper estuary. The maximum high water line of Rilo et al. (2014), where available, is represented in blue, and the dikes in black. The red lines in b) represent stretches of the dikes that were overtopped during the 2010 Xynthia storm. The yellow circles indicate atmospheric stations. Real and virtual tidal gauges are represented as red circles.

Measured tidal ranges vary between 0.55 m and 3.86 m at the coast (Guerreiro et al., 2015) but resonance significantly amplifies the semi-diurnal tidal constituents within the estuary (Fortunato et al., 1999). Simultaneously, the estuary is strongly ebb-dominated due to the large extent of the tidal flats (Fortunato et al., 1999). The estuary is usually partially mixed, although it can be stratified when neap tides are combined with high river discharges (Neves, 2010).

The impact of storm surges and waves on the Tagus estuary dynamics is poorly studied. Canas et al. (2009) found atmospheric pressure to be more important than wind in determining the surge within the estuary. Oliveira (2000) applied a wave model to the estuary mouth and found that short waves were dissipated in the ebb-delta sand bars at the entrance of the estuary. Rusu et al. (2011) analyzed the effect of tidal currents on wave propagation at the Tagus estuary mouth, and found the currents to increase the significant wave height and the mean wave period on ebb and decrease them on flood. Inside the estuary, locally-generated waves can reach significant wave heights of 0.8 m. This value was measured between Cacilhas and Seixal (Figure 2a) during a storm event with winds of about 11 m/s (Freire et al., 2009), and simulated by Rusu et al. (2009) for winds of 12 m/s.

Included in the Lisbon Metropolitan Area, the estuary comprises along its margins 11 municipalities with about 1.6 million of total inhabitants, mostly concentrated in its western and northern sides (Tavares et al., 2015). This densely urbanized water front contrasts with a large extension of productive agricultural areas on the eastern side of the estuary (known as “Lezíria”) and along the three islands formed by alluvial deposition (from South to North: Póvoa, Lombo and Alhandra, Figure 2b). The distinct occupation of the estuary right and left margins is also associated to markedly different topographies. In general, the right margin exhibits a high relief, whereas the left margin is characterized by extensive lowlands. The estuary also hosts a natural reserve (the Tagus Estuary Natural Reserve) that is one of the most important sanctuaries for birds in Europe, covering about 14,000 hectares.

The detailed land-use cartography of the estuarine fringe (defined by the Portuguese law as the 550 m wide fringe above the water line at the highest astronomical tide), which covers a total area of 130 km^2, shows that the most important occupation types are the agricultural (35%) and the urban (34%) zones, with smaller contributions of industrial, port and airport facilities (24%), green spaces (6%) and natural areas (1%) (Rilo et al., 2012).

2.2. The 1941 and the 2010 Xynthia storms’ impacts

The most severe wind storm to have hit the Iberian Peninsula in the 20th century made landfall in the Portuguese coast on February 15th, 1941 (Freitas and Dias, 2013) coming from the SW (Figure 1). The atmospheric pressure dropped 45 hPa in 18 hours over Portugal (Ganho, 2013), thus it was an explosive cyclogenesis, reaching minimum values of 952.1 hPa at the Geophysical Institute in Lisbon and 957.8 hPa in Monte Estoril (Figure 2a). The wind speed reached almost 20 m/s at the same stations, although these values may underestimate the maximum wind speed over the water due to resistance imposed by the urban environment. The wind bursts in Lisbon reached 38 m/s (Nunes et al., 2012). The information about the river flow is scarce. A major river flood occurred in the Tagus River a few weeks earlier, on January 23-25, and flood marks indicate that it led to the second worst inundation on record in the Lezíria. This was the 4th largest flood recorded at Vila Velha de Rodão (located in the Tagus River near the border between Portugal and Spain, about 200 km from the estuary mouth) since the mid-

nineteenth century (Salgueiro et al., 2013), so the river flow was likely still high when the February storm hit the coast. The daily-mean river discharge at Vila Velha de Rodão (the hydrological station closest to the estuary at that time) peaked at 3266 m^3/s on February 16. This river flow corresponds to a return period of about 3 years, according to the Tagus watershed management plan. Finally, although a tide gauge was already in operation at Cascais, measurements are unavailable between the 13th and the 15th of February due to malfunction. The tidal range obtained from a harmonic synthesis is 3.0 m (Table 1). This value corresponds to 78% of the maximum tidal range, and to the percentile 91 of the tidal ranges. Wave data are unavailable, but a newspaper cited by Freitas and Dias (2013) mentions 20 m waves in the Tagus estuary. While this value cannot be confirmed, it suggests that wave heights were totally uncommon and probably extremely high.

The margins of the Tagus estuary were severely hit. Overall, the human losses in the estuary include 28 casualties, 14 wounded, 125 evacuees and 3 displaced (Freire et al., 2016). Freitas and Dias (2013) report flooding in downtown Lisbon, destruction of workshops and warehouses in the harbor, dozens of smashed boats, many sank ships (150, according to Nunes et al., 2012) and the interruption of the railway between Lisbon and Cascais. Similarly, flooding occurred in Cascais causing severe damage. The walls protecting the northern margin of the estuary upstream of Pedrouços were destroyed (Nunes et al., 2012). In the upper estuary, houses in Alhandra were flooded with more than 1 m of water, and 25 of its inhabitants drowned (Muir-Wood, 2011). Since this town is located on the margins of the Tagus estuary across from the Lezíria, it is expected that the Lezíria itself was flooded as well. According to local reports (Companhia das Lezírias, 1941, cited in Madaleno, 2006), this storm destroyed all the channels and dikes in the Lezíria.

A storm following a similar SW-NE path but clearly less intense over the study area, Xynthia, struck the Portuguese coast on the morning of February 27th 2010 (Figure 1; Liberato et al., 2013; Breilh, 2014). Xynthia became known for causing extreme flooding in the central part of the Bay of Biscay on the dawn of February 28 (Bertin et al., 2012). However, in Portugal, Xynthia was less severe than the 1941 storm and the tidal range (2.9 m) was lower. Like in 1941, the storm coincided with a spring tide, exacerbating its consequences. In the days preceding the storm landfall the river flows were high, and floods are reported in riverine towns, such as Santarém (http://otejo.com/2010/02/25/, last accessed on July 11, 2016). During the storm and in the following days, inundations occurred in several places in the Tagus estuary (Freire et al., 2016) and the Aveiro Lagoon (Lopes, 2016) but no casualties were reported. In the Lezíria, there is evidence of flooding during the 2010 February-March storms (Figure 2b). During three consecutive days, witnesses report that the dikes were overflown during the night and dawn. The dikes that were overflown and damaged during the storm were later repaired and raised. Inundations in the Tagus estuary also occurred in the Seixal downtown area. Freire et al. (2016) determined the extent of the inundation in this area through interviews and photographs. The similarities between the two storms (Figure 1 and Table 1) make Xynthia an excellent case to validate the ability of the model to reproduce storm events and, in particular, to reproduce the extent of inundation.

Table 1. Characteristics of the two storms. The tidal range is computed from the results of the tidal model of Fortunato et al. (2016) at Cascais.

Storm	Tidal range (m)	Minimum atmospheric pressure (hPa)	Maximum wind speed (m/s)	River flow
1941	3.0	952.1 (Geophysical Institute) 957.8 (Monte Estoril)	18 (Geophysical Institute) 19 (Monte Estoril)	There was a major river flood in January 21-23. River flow in the Tagus river peaked at 3266 m^3/s at Vila Velha de Rodão.
2010	2.9	976.2 (Lisbon) 986 (Cascais)	14 (Lisbon)	River flow in the Tagus river peaked at 3917 m^3/s on February 27 at Almourol

3. DATA

3.1. Bathymetry and topography

The extreme water levels in an estuary and the extent of an inundation largely depend on the bathymetry and topography. The generation of a digital terrain model was thus a very sensitive task. The lack of a comprehensive, detailed and updated dataset led to the use of multiple sources of data. These sources are briefly described below. The digital terrain model interpolated onto the finite element grid described below is shown in Figure 2.

The only comprehensive bathymetry of the estuary dates back to 1964/67. This dataset was used as a baseline bathymetry and updated wherever possible. In most of the navigated areas (channels and docks) and in the tidal inlet, recent bathymetries were made available by the Lisbon Harbor authority. Topographic data along the margins of the estuary and LIDAR (Light Detection and Ranging) data along the coastal margins, both from 2011, were provided by the Portuguese Environment Agency and the Portuguese institution in charge of the geographical information (*Direção-Geral do Território* - DGT), respectively. Upstream of Vila Franca, only cross-channel survey data were available. Since the distance between transects (2.5 km) prevents the direct interpolation of the bathymetry, the mean cross-sectional area was evaluated and a linear regression was determined along the axis of the estuary (Figure 3). This regression was then used to interpolate the depths along the riverine part of the domain. Similarly, the spacing between available cross-sectional data along the upper Sorraia River varies between 200 and 1500 m. Given the narrow width of this part of the river it was represented with a rectangular cross-section and the bathymetry was interpolated using available cross-sections. The depth along the Risco River was estimated based of the few data points available.

The topography of the margins was mostly based on a 2008 dataset provided by DGT and obtained by aerial photogrammetry. Although this dataset was provided on a 2 m resolution grid, there are some doubts on the accuracy of the dikes' crest heights. The height of the crest of the dikes protecting the Lezíria was provided by a farmers' association (*Associação dos Beneficiários da Lezíria Grande de Vila Franca de Xira*) and verified in a few places by a dedicated topographic survey. The dikes covered by this dataset extend from the margins of the Sorraia River to the Tagus River. These data were measured after the partial reconstruction of the dikes that followed their damage during the Xynthia storm. The dikes represented in the model are therefore higher than the ones that existed during the Xynthia storm.

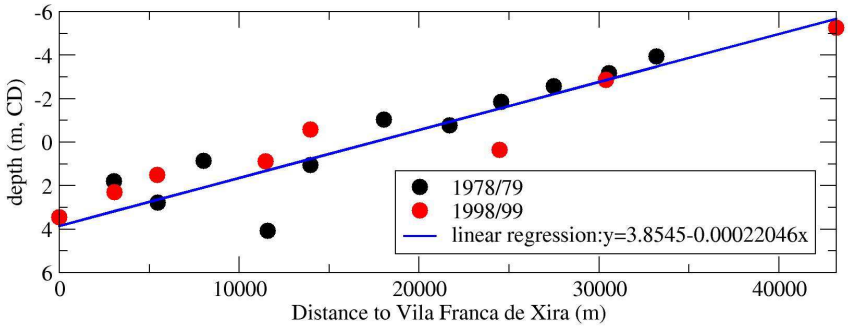

Figure 3. Determination of cross-sectional-averaged depth along the estuary axis upstream of Vila Franca. CD stands for Chart Datum.

3.2. Dynamic data

Atmospheric pressure measurements from 1941 at two stations in the Tagus estuary region were provided by the Portuguese Institute for Sea and Atmosphere. Pressure dropped to 952.1 hPa in Lisbon (Table 1) and is used below to validate the atmospheric model.

Water levels were measured at 13 tidal gauges installed along the estuary in 1972. These time series were harmonically analyzed to extract the amplitudes and phases of the tidal constituents (Fortunato et al., 1999). Time series for model validation are obtained by harmonically synthetizing the tidal elevations using the same constituents included in the model.

Daily averaged river flows measured at Vila Velha de Rodão in 1941 are available from the Portuguese water resources information system (www.snirh.pt). However, this station is located over 100 km upstream of the estuary. The estimate of the river flow at the model boundary took into consideration that: 1) the peak river flow at Vila Velha de Rodão at the time of the storm, of the order of 3500 m^3/s, corresponds to a return period of about 3 years; 2) for that particular return period, the river flow at the estuary's head (station of Almourol) is 4600 m^3/s, i.e., about 30% higher. Hence, the river flow at the estuary's head was estimated as 30% higher than the one measured at Vila Velha de Rodão (Figure 4). Cubic splines were used to obtain a smooth time series.

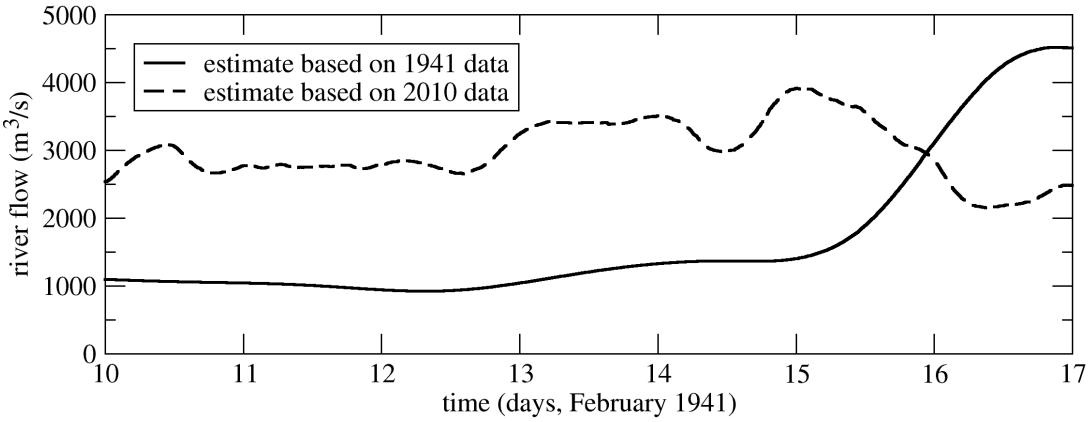

Figure 4. Estimates of the river flow reaching the estuary.

After 1941, several dams were built in this watershed and the reservoir capacity in the Spanish territory now exceeds the average annual water resource volume (Salgueiro et al., 2013). As a result, the same meteorological conditions that occurred in February 1941 would lead to a different river flow nowadays. Hence, an alternative approach to estimate the river flow was followed. Since the trajectories of the February 1941 and the 2010 Xynthia storms were fairly similar, the river flow for the 1941 storm was estimated as the river flow measured at Almourol (about 40 km upstream of the grid boundary) during the Xynthia storm.

Both approaches followed to estimate the fresh water flow have clear limitations: the first approach ignores the changes in the watershed between 1941 and today, as well as the time lag between the river flow at the Spanish border and the model boundary; the second approach assumes that precipitation was similar in the two events. Not surprisingly, the river flows estimated by the two approaches show significant differences, even though the order of magnitude is the same (Figure 4). Hence, a sensitivity analysis of the model results to the choice of the river flow time series is performed below.

Finally, since there are no measurements of river flow in the Sorraia River for the relevant period, this river flow is taken as 5% of the river flow in the Tagus River, based on the ratios between annual averages in the two rivers.

4. NUMERICAL MODELS: DESCRIPTION, APPLICATION AND VALIDATION

4.1. Atmospheric model

The atmospheric conditions over the North Atlantic region favoring the explosive development of the 15 February 1941 winter storm were simulated using the mesoscale Weather Research & Forecasting Model - Advanced Research model (WRF-ARW) version 3.5 (Skamarock et al., 2008). For this experiment, the initial and boundary conditions for the large-scale atmospheric fields of pressure, wind, humidity and temperature, as well as initial soil parameters (soil water, moisture and temperature) and sea surface temperature, are given by the 2-degree horizontal resolution 20th Century Reanalysis (20CRv2, Compo et al., 2011).

In order to obtain a good representation of the complete genesis and development of the storm, a two-way interactive nested domains configuration was setup: a parent domain with a 27 km horizontal resolution and a child domain with 9 km horizontal resolution. The outer domain covers an area that includes both the North Atlantic basin extension from the Gulf Stream region to the Iberian Peninsula and most of the subtropical North Atlantic Ocean (Figure 1). Both domains have 32 vertical unequally-spaced levels, with the model top at 50 hPa. Further details on the simulation of explosive developing storms in the North Atlantic are presented in Ferreira et al. (2016).

The main physical parameterizations applied herein to all domains follow the work of Ferreira et al. (2014) who performed a sensitivity test to 24 combinations of physical parameterization schemes (short wave radiation, cumulus, microphysics and surface-planetary boundary layer) in 36 periods during 2006, comparing model results of temperature, mean sea level pressure, humidity and wind speed with observations along the continental Portuguese area. Thus the parameterization setup used in the present study includes the WRF Single-Moment 6-class

microphysics scheme (Hong and Lim, 2006), Duhdia shortwave radiation (Dudhia, 1989), the Rapid Radiative Transfer Model (RRTM) longwave radiation model (Mlawer et al., 1997), the Noah Land Surface Model (Chen and Dudhia, 2001), the Yonsei University (YSU) boundary layer parameterization (Noh et al., 2003) and the Grell-3D scheme (Grell and Devenyi, 2002).

The 20CRv2 dataset provides atmospheric data from 56 ensemble members. For this research a sensitive analysis was made and the atmospheric downscaling was performed to a member of the 20CRv2 reanalysis closer to the pressure evolution observed at the Lisbon meteorological station and corresponded to the member that predicted the most intense storm. The simulation period was between 00 UTC 10/02/1941 and 00 UTC 17/02/1941.

The simulations are validated with observational pressure data available at the Lisbon and Estoril meteorological stations (Figure 5). The simulated pressure evolution on both positions follows the observed values, including the pressure drop on the deepening phase of the cyclone. However it underestimates the maximum intensification and weakening phase of the storm. Considering that the reanalysis data are obtained without radiosondes information, the vertical structure of the conditions during the storm are expected to introduce some errors that for such nonlinear systems affect the evolution of the storm.

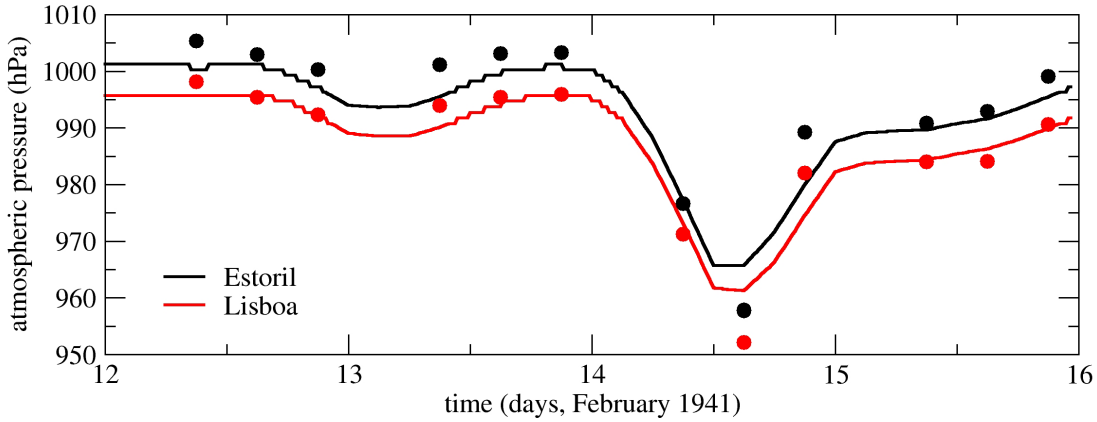

Figure 5. Validation of the atmospheric model: comparison between the measured (circles) and modeled (lines) atmospheric pressures.

4.2. Regional-scale wave model

Time series of directional energy spectra were computed from a regional application of the WaveWatchIII model (Version 3.14; Tolman, 2009), implemented over the North Atlantic Ocean with a 0.5° resolution (Figure 1). The spectral space was discretized using 24 equally-spaced directions and 24 exponentially-spaced frequencies spanning 0.04-0.4 Hz. Sea-ice at high latitudes was taken into account according to the procedure described in Bertin et al. (2013). The source terms associated with wind input and dissipation by whitecapping were computed using the parameterization Cycle4 described in Bidlot et al. (2007). Further details on the model application and validation are provided in Bertin et al. (2013). The model was forced with time series of wind fields originating from the dynamic downscaling of the 20CRv2 reanalysis described above.

Because the validation of the wave model presented in Bertin et al. (2013) focuses on yearly-mean discrepancies, this hindcast was compared against measured wave heights at Leixões and Sines, two stations for which have pluri-annual time series are available (Figure 6). This comparison reveals Root Mean Squared Discrepancies (hereafter RMSD) of 0.32 and 0.38 m, which yield normalized errors of 16 to 24% respectively. Arbitrarily focusing on wave heights larger than 4 m, these errors drop to 13 and 19% respectively, with normalized biases smaller than 5%.

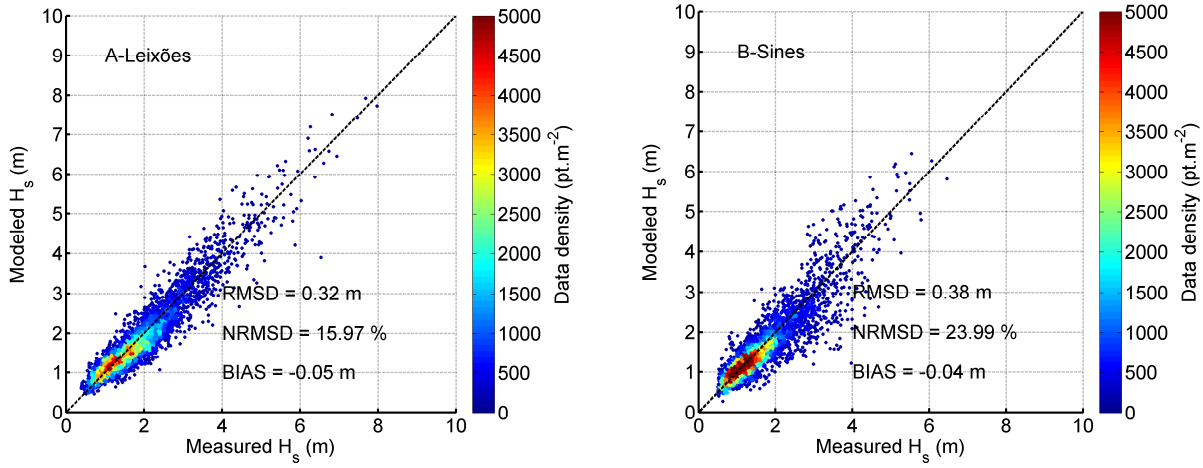

Figure 6. Validation of the significant wave heights obtained with the regional wave model at Leixões and Sines, respectively to the North and to the South of the Tagus estuary, for the period 2007-2012. RMSD: root mean square deviations; NRMSD: normalized root mean square deviations.

4.3. Regional scale tide and surge model

Simulations of tides, surges and waves are performed with the modeling system SCHISM (Zhang et al., 2016). SCHISM (*Semi-implicit Cross-scale Hydroscience Integrated System Model*) is a derivative product built from the original SELFE model (v3.1dc; Zhang and Baptista, 2008), with many enhancements and upgrades including an extension to large-scale eddying regime and a seamless cross-scale capability from creek to ocean (Zhang et al. 2016). SCHISM uses semi-implicit finite elements and finite volume methods, combined with Eulerian-Lagrangian methods, to solve the shallow water equations. SCHISM is also fully parallelized. It includes modules for surface waves (Roland et al., 2012), morphodynamics (Pinto et al., 2012; Guérin et al., 2016) and water quality (Rodrigues et al., 2009, 2011; Azevedo et al., 2014).

SCHISM was applied in 2D depth-averaged mode to the NE Atlantic (Figure 1). The model is forced by tides from a global tide model (Finite Element Solution - FES2012, Carrère et al., 2012), winds and atmospheric pressure from the WRF-ARW application described above, and tidal potential. Eleven tidal constituents are imposed inside the domain through the tidal potential, and twenty nine tidal constituents are forced at the boundary. The grid has about 150,000 nodes and a resolution of about 250 m at the Portuguese coast. The time step is set to 5 minutes. A detailed description of the model application and validation is presented in Fortunato et al. (2016).

4.4. Local scale tide, surge and wave model

The circulation and wave propagation in the Tagus estuary were simulated with the coupled model SCHISM-WWM (Roland et al., 2012) in depth-averaged mode. Two-way coupling is important, as there is a significant modulation of waves by tidal elevation and currents at the mouth of the Tagus estuary (Rusu et al., 2011). The model was forced by wind and atmospheric pressure from the WRF-ARW simulation, time series of wave spectra from the WW3 simulation, elevations and velocities from the SCHISM simulation and river flows. Radiation stress gradients and wind stresses computed by WWM are used to force the shallow water model, and both elevations and velocities from SCHISM are used in the solution of the wave action equation in WWM. Detailed descriptions on the coupling between SCHISM and WWM are given in Roland et al. (2012) and Schloen et al. (2017).

The grid was generated with the softwares *xmgredit* (Turner and Baptista, 1993) and *nicegrid* (Fortunato et al., 2011), based on grids from previous applications (Guerreiro et al., 2015, Fortunato et al., 2017). The domain is over 110 km long and has a surface area of 1442 km^2. It extends from the ocean, 27 km away from the estuary mouth, to the river, and includes the agricultural flood-prone areas in the northeastern part of the estuary (Figure 7a). The primary generation criterion was the detailed representation of the geometry. The narrow channels have a finer resolution, to allow the proper propagation of the tide. Nodes and element sides were placed along the crests of the dikes (Figure 7b), to optimize the representation of the elevation of these sub-grid-scale features (Bilskie et al., 2015). The resulting grid has 140,000 nodes and a resolution between 2 and 800 m (Figure 7a). The time steps were set to 1 minute for SCHISM and 15 minutes for WWM.

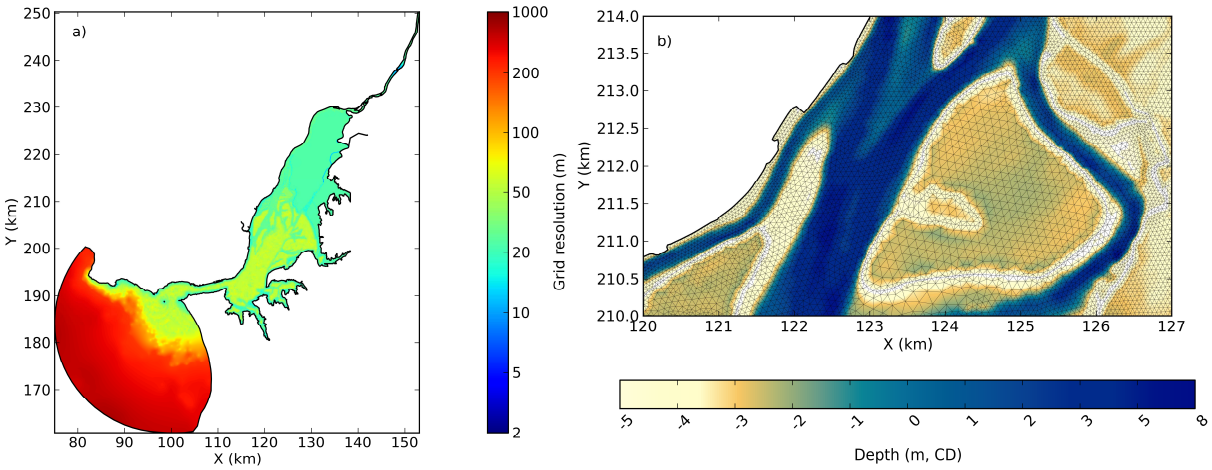

Figure 7. Model grid: a) model domain and grid resolution; b) detail of inundation-prone areas of the upper estuary.

Friction was parameterized using a Manning coefficient (Figure 8). This coefficient was selected based on previous experience (Guerreiro et al., 2015), the nature of the estuary bottom and the land cover. In particular, the Manning coefficient was taken as 0.015 m$^{1/3}$/s in the upper Tagus estuary, where the bottom sediments are muddy. In contrast, values of up to 0.027 m$^{1/3}$/s were used in the Tagus River, whose bottom sediments are primarily sands. In the dry areas, the Manning coefficient was determined based on the land cover from Chen et al. (2015).

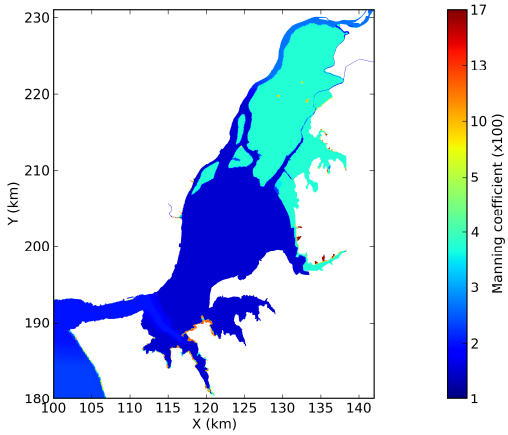

Figure 8. Manning friction coefficient ($m^{1/3}/s$).

The model's ability to simulate tidal propagation was validated first. A one-year simulation was performed, forced by tides from the regional model of Fortunato et al. (2016) at the ocean boundaries and by average river flows of 517 m^3/s and 20 m^3/s at the Tagus and Sorraia boundaries, respectively. Biased and unbiased root mean square errors were computed at 13 stations (Table 2). Errors compare favorably with those obtained in previous applications with the same dataset (Guerreiro et al., 2015). Unbiased root mean square errors at high tide were also computed, to assess the model's ability to represent high water levels. Results show that the model reproduces high tides with errors between 10 and 20 cm in the upper estuary (Table 2).

Table 2. Errors in the Tagus for the 1972 validation run (in cm).

Station	RMSE	U-RMSE	HT-RMSE
Cascais	4.6	4.6	5.7
Paço de Arcos	6.4	3.8	4.6
Trafaria	9.7	5.4	7.7
Lisbon	11.0	6.1	13.5
Pedrouços	6.3	4.0	7.4
Cacilhas	5.8	5.3	6.0
Seixal	8.9	6.4	8.9
Montijo	12.4	6.6	13.8
Cabo Ruivo	14.5	8.6	15.4
Alcochete	11.7	10.4	9.2
Santa Iria	16.0	12.8	15.0
Ponta da Erva	16.8	16.7	10.5
Vila Franca	18.5	9.9	19.5

The ability of the model to reproduce flooding during an extreme event was verified by simulating the inundation of the Seixal downtown area during Xynthia, since the inundation limits were available at this location. In this case, the atmospheric model was initialized by results from Interim Reanalyses (ERA-Interim) as obtained from the European Centre for Medium-Range Weather Forecasts Reanalysis (ECMWF). ERA-Interim is the latest ECMWF global atmospheric reanalysis available since 1979 up to the present (Dee et al., 2011). Results show that the

model represents inundation accurately, within the limits of grid resolution (Figure 9): ten out of 16 points determined as the limits of inundation fall in the stripe identified by the model as the inundation limit, four other points fall in the last row of wet elements, one point is located in the second row of wet elements and one point is in the dry area. For the same period (February 25 to March 3, 2010), the root mean square elevation error at the Cascais tide gauge is 7.5 cm.

Figure 9. Validation of the modeled inundation of the Seixal downtown area during Xynthia. The red circles represent the inundation limits determined in the field and the blue shape is an interpretation of the inundated area based on those limits and the existing buildings (from Freire et al., 2016). Dark (light) green triangles represent fully (partially) wet elements as determined by the model. Fully dry elements are omitted for clarity.

In spite of the good results provided by the validation exercises, some uncertainty remains on the results. Sensitivity analyses were therefore performed on some perceived weaknesses of the model. The errors introduced by the grid resolution were assessed by running the model with a finer grid. In Run 2 (Table 3), all elements were split into four, while preserving the bathymetry. The importance of the uncertainty associated to the river flow was assessed by forcing the model with the river flow measured during Xynthia (Run 3). Finally, the default values of the friction coefficient (0.067 m^2/s^3) and the wave breaking coefficient (0.78) were used in the wave model. The first value is adequate for fully developed wind seas (Bouws and Komen, 1983), but may be too large for swell dissipation over sandy bottoms (Hasselman et al., 1973), as is the case here. Therefore, a smaller friction coefficient (0.038 m^2/s^3) was used in Run 4. Similarly, the wave breaking coefficient typically takes values between 0.6 and 0.78. Therefore, a simulation with the lower value was also conducted (Run 5).

Table 3. Model simulations

Run	Open boundaries				Surface boundary		Processes	Other
	Tide	Surge	Waves	River flow	Wind	Atmospheric pressure gradient	Wave generation	
1	1941	Yes	Yes	1941	Yes	Yes	Yes	–
2	1941	Yes	Yes	1941	Yes	Yes	Yes	Fine grid
3	1941	Yes	Yes	2010	Yes	Yes	Yes	–
4	1941	Yes	Yes	1941	Yes	Yes	Yes	Reduced friction in WWM
5	1941	Yes	Yes	1941	Yes	Yes	Yes	Reduced breaking coefficient in WWM
6	2006	Yes	Yes	1941	Yes	Yes	Yes	–
7	1941	Yes	Yes	1941	Yes	Yes	Yes	SLR
8	1941	No	No	Climatology	No	No	No	–
9	1941	No	Yes	1941	Yes	Yes	Yes	–
10	1941	Yes	No	1941	Yes	Yes	Yes	–
11	1941	Yes	Yes	Climatology	Yes	Yes	Yes	–
12	1941	Yes	Yes	1941	No	Yes	Yes	–
13	1941	Yes	Yes	1941	Yes	No	Yes	–
14	1941	Yes	Yes	1941	Yes	Yes	No	–
15	M2	No	Constant	Constant	No	No	No	–
16	M2	No	No	Constant	No	No	No	–
17	1941	Yes	Yes	1941	Yes	Yes	Yes	Dikes raised by 20 cm

The sensitivity of the model was assessed through the maximum water elevations obtained at several tide gauges (Table 4). The station of Cascais was not used. It is located inside a marina, in an area with steep rocky slopes, and the grid resolution is inadequate to properly represent wave breaking. Instead, two stations were considered on both sides of the estuary mouth: Carcavelos and São João (Figure 2). These stations were placed at a depth equal to the mean sea level. Results at these stations are only representative of the region for the same depth, as moving these stations in the cross-shore direction can change the water level by tens of centimeters. Results were also examined at Conchoso, the approximate limit of salinity intrusion under drought conditions (Rodrigues et al., 2016).

In general, the differences between the four simulations are of the order of a few millimeters (Table 4), thereby providing confidence in the results. The maximum differences occur at the edges of the estuary, where they can reach a few centimeters. Refining the grid increases the maximum water level at Conchoso by 5 cm, suggesting that the standard grid may be too coarse in the riverine portion of the domain. Similarly, forcing the model with the river flow from 2010 increases the maximum water level at the same station by 10 cm. These two results suggest that the model may underestimate the extreme water levels and thus the inundation in the upstream part of the domain. However, this problem appears to be localized since the sensitivity of the model at the following downstream station (Vila Franca) is modest. At the coast

(Carcavelos and São João) the model exhibits some sensitivity to the friction coefficient of the wave model. However, the sensitivity of the model results inside the estuary to this coefficient is negligible. The sensitivity to the wave breaking coefficient is also negligible.

Table 4. Maximum elevations for the sensitivity analysis simulations (m, CD). For each of the runs 2-5 the values representing the maximum discrepancy relative to Run 1 are highlighted in bold.

Station	Run 1 (standard)	Run 2 (fine grid)	Run 3 (river flow)	Run 4 (reduced friction)	Run 5 (reduced breaking coef)
Carcavelos	4.787	4.786	4.787	**4.798**	4.787
São João	4.780	4.779	4.781	**4.791**	4.780
Paço de Arcos	4.506	4.502	4.505	4.506	**4.513**
Trafaria	4.597	4.598	4.604	4.599	4.597
Lisbon	4.592	4.591	4.599	4.593	4.592
Pedrouços	4.721	4.739	4.726	4.723	4.721
Cacilhas	4.735	4.755	4.742	4.736	4.735
Seixal	4.777	4.803	4.782	4.779	4.776
Montijo	4.832	4.854	4.830	4.833	4.831
Cabo Ruivo	4.873	4.900	4.876	4.875	4.874
Alcochete	5.013	5.035	5.014	5.015	5.013
Santa Iria	5.100	5.122	5.099	5.103	5.100
Ponta da Erva	5.150	5.121	5.158	5.155	5.152
Vila Franca	5.377	5.387	5.368	5.538	5.376
Conchoso	5.588	**5.640**	**5.685**	5.589	5.590

4.5. Scenarios

Several inundation scenarios were considered. Scenario 1 (Run 1, Table 3) assumes that the 1941 storm would occur in 2016, i.e., considering the 2016 mean sea level (2.26 m above the Chart Datum, CD).

Scenario 2 (Run 5, Table 3) is a “worst case” scenario, in which the 1941 storm is combined with a high tidal range. The largest predicted tide in a 20 year period (2001-2020) was selected. It occurred on March 1st 2006 and had a tidal range of 3.6 m.

Finally, scenario 3 (Run 6, Table 3) takes into account climate changes predicted for the end of the 21st century. Contrary to some areas of the world, the Portuguese coast is not experiencing an increase in storminess. Almeida et al. (2011) did not find any evidence of a change in storminess in the Portuguese south coast between 1952 and 2009. Marcos et al. (2011) suggested that the storm surges in the Iberian coast will decrease slightly in the future. Vousdoukas et al. (2016) reached a similar conclusion for southern Europe and for most climate scenarios. These results are in agreement with the ones obtained for the winter extra-tropical cyclone activity, over this region, where no statistically significant signal is found neither considering all cyclones nor only the most severe systems (Ulbrich et al., 2013). Hence the only change considered herein is the mean sea level rise (SLR).

Several values have been proposed for the SLR by the end of the 21st century. Antunes and Taborda (2009) projected a SLR of 0.47 m between 1990 and 2100 based on data from the Cascais tide gauge. Lopes et al. (2011) estimated a local sea level rise of 0.42 m between 1980-1999 and 2091-2100 using results from a climate model for scenario SRES-A2. Also, analyses

of the Cascais tide gauge data indicate that the SLR rate is consistent with global estimates: for instance, the mean sea level rose by about 0.15 m in the 20th century (Antunes and Taborda, 2009). This consistency may be due to the negligible vertical movement of the area: GPS-based methods indicate that this area has an upward vertical movement which is an order of magnitude smaller than SLR (www.sonel.org/spip.php?page=gps&idStation=648.php). The agreement between the SLR at Cascais and the global values justifies the use of global estimates of SLR (Guerreiro et al., 2015). The most recent estimates of the mean SLR for the end of the 21st century vary between 0.37 and 0.82 m (IPCC, 2013). Therefore, we adopted the value of 0.5 m as a suitable representative value of SLR between present (2016) and the end of the century.

5. RESULTS AND DISCUSSION

5.1. Regional scale atmospheric and oceanographic behavior

Reanalysis data and simulations used for the assessment of the synoptic evolution and dynamical characteristics of the 1941 windstorm allow retrieving the developing cyclone at 00 UTC 15 February on the subtropical North Atlantic near 20ºW and 35ºN (Figure 1). From this location it experienced a notorious strengthening with a deepening rate over 22 hPa/12h, a value that after geostrophic adjustment to the reference latitude of 60˚N increases to 32 hPa/12h, showing how exceptional this event was. In the upper levels of the model grid a meandering, intense jet stream (over 70 m/s at 250 hPa) triggered and propelled the storm to the northeast, similarly to Xynthia (Liberato et al. 2013). The storm made landfall 12 hours later in the north of Portugal, some 350 km to the north of the Tagus estuary. Maximum winds close to 30 m/s hit the south of Portugal coming from the South and Southwest. The cyclone then crossed the Iberian Peninsula and moved northeast, heading to the Bay of Biscay and then to the British Islands, where it weakened.

As previously noted, the 1941 and 2010 Xynthia storms have similar trajectories and lifecycles, though the former storm was even more intense. The reduced number of such extreme cyclones affecting the Iberian Peninsula prevents the establishment of a return period for these events. However, a climatological assessment to characterize the large-scale atmospheric conditions and cyclone tracks during the top-100 potential socioeconomic losses over Iberia associated with wind events, based on 65 years of reanalysis data from the National Centre for Environmental Prediction/National Centre for Atmospheric Research, showed that the lowest minimum mean value for the event day (±1 day) was 966 hPa (Karremann et al., 2016). This analysis indicates that the return period of the 1941 storm is probably higher than 65 years.

The cyclonic winds generated energetic waves to the south of the cyclone's track directed to the north-east, moving to the Portuguese coast. The highest waves, with significant wave heights of 13-14 m and peak periods around 14 s, hit the coast close to the Tagus estuary mouth. These significant wave heights are exceptional, with a return period of over 100 years (Figure 10a). In contrast, the north of Portugal was hit by smaller waves, with return periods below 10 years.

In spite of the severity of the storm and resulting waves, the maximum elevations at the coast are relatively modest. The maximum elevations at the western Iberian coast (neglecting the wave setup) correspond to return periods varying between 2 years in the south and 20 years in

the north (Figure 10b). This result is explained by the low tidal amplitude, which corresponds only to the percentile 91 of tidal ranges. The growth of the return period from the South (where onshore winds are maximal) to the North (where the atmospheric pressure is minimal) is consistent with the higher importance of the atmospheric pressure relative to the wind in the generation of storm surges in this region. Indeed, the effect of wind stress on the storm surge decreases with increasing water depth. Since the Portuguese continental shelf is very narrow, the wind setup is modest even for very strong winds.

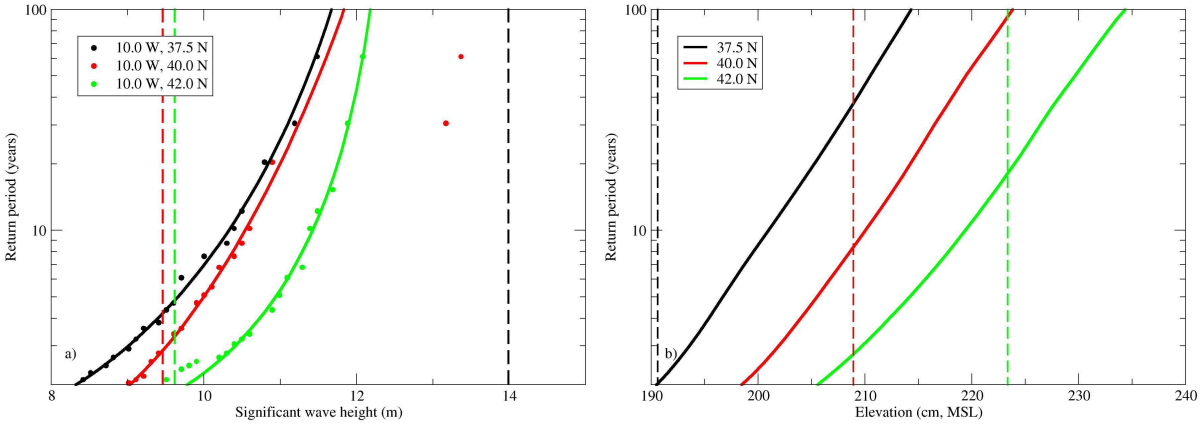

Figure 10. Return period of the 1941 storm effects along the Portuguese west coast. The vertical dashed lines indicate the value reached in the 1941 simulation at three different latitudes indicated by the color. a) Return periods of the significant wave height based on the 1952-2012 hindcasts of Bertin et al. (2013). The solid lines are a GEV distribution fitted to the empirical distribution (circles). b) Return periods for the maximum elevations at the Portuguese west coast based on the 1980-2010 hindcasts of Fortunato et al. (2016), and computed with the approach of Fortunato et al. (2013). These return periods do not take wave setup into account.

5.2. Inundation in the Tagus estuary

The maximum water level obtained at Cascais in Run 1 (hence including wave setup) is 2.08 m relative to present mean sea level. Considering the analysis of extreme water levels based on data from the same station (Guerreiro et al., 2015), this water level corresponds to a return period of just over 20 years. This return period is significantly higher than those obtained in Figure 10b at the two points to the South and North of Cascais (about 2 and 10 years, respectively). This contrast shows that the waves that occurred in 1941 significantly contributed to the storm surge.

Results show that a storm similar to the 1941 event could cause today some inundation of the SW area of the Lezíria (Figure 11a), and that the extent of the inundation would be higher than during Xynthia (Table 5). The portion of the dike that was overflown during Xynthia, to the North of the Lombo Island, would be overflown again, even though the crest was raised by about half a meter after the Xynthia event. However, the flooded area would be small (1.6 km^2, Table 5) due to the presence of a second dike (Figure 2b). The islands of Póvoa and Alhandra would be flooded as well. On the left margin of the Sorraia River, an area of about 18 km2 would be flooded due to the discontinuity and low height of some of the dikes.

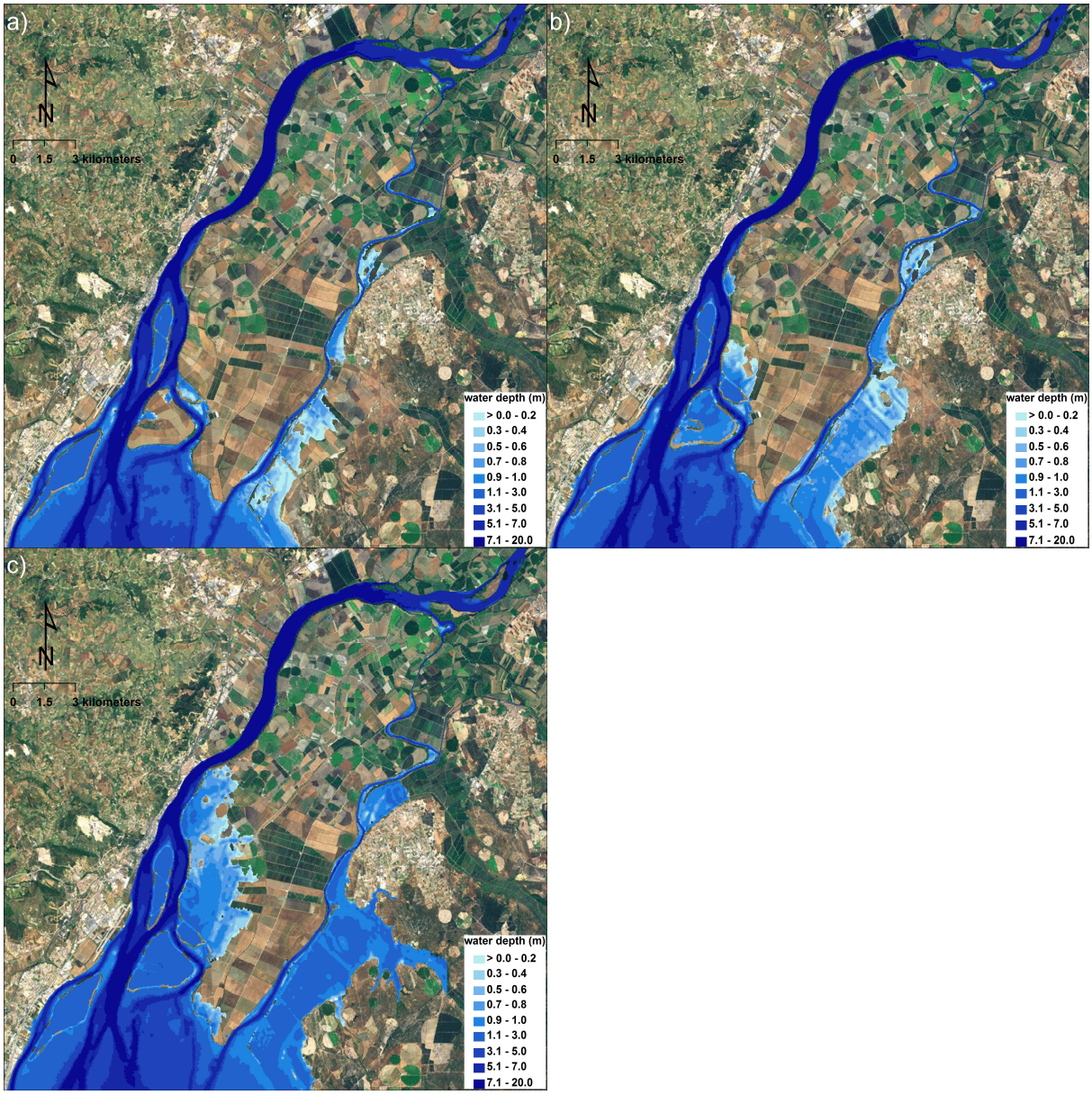

Figure 11. Inundation of the upper Tagus estuary for the 1941 storm: a) present MSL; b) worst case scenario, obtained by combining the 1941 storm with an extreme spring tide; c) sea level rise of 0.5 m.

The reliability of these results may be limited by the available topographic data, which may be particularly inaccurate around the dikes' crests. To assess the sensitivity of the results, an additional simulation (Run 17, Table 3) was performed in which the height of the dikes' crests was uniformly raised by 20 cm. Results indicate that, in most areas, the inundation extent is not very sensitive to errors of this magnitude, thereby providing further confidence in the estimated inundation areas (Table 5). A related source of uncertainty is the dikes' erodibility, which was not considered in the simulations. The dikes are fragile and require frequent repairs. For instance, in

May 2016 a small breach occurred in one of the dikes that protect the Póvoa Island and rapidly grew over the following months. As a result, a significant portion of the island became frequently flooded. In the case of an extreme event, it is likely that the dikes would give in at some places (as was the case during Xynthia), further exacerbating the inundation.

Table 5. Inundated areas (km^2).

Zone	Run 1	Run 6	Run 7	Xynthia (2010)	Run 17
Lezíria	1.6	2.5	25.2	1.1	1.3
Póvoa island	4.1	4.2	4.2	4.1	4.1
Lombo island	0.8	4.9	5.1	0.1	0.1
Alhandra island	2.4	2.5	2.5	0.1	1.4
Sorraia left margin	17.9	27.7	40.1	10.1	14.3

The inundation extent would increase if the tidal amplitude was higher (Figure 11b). In this case, the extreme water level at Cascais increases to 2.39 m relative to present mean sea level, which corresponds to an estimated return period above 1000 years. The second dike in the Lezíria would be overflown increasing the flooded area to 2.5 km2, all three islands would be flooded, and the inundated area in the Sorraia left margin would increase by over 50%.

Finally, if the 1941 conditions are combined with a 0.5 m rise in mean sea level, the problem would be significantly aggravated (Figure 11c). Almost 80 km2 of land would be flooded, in spite of the presence of the dikes.

5.3. Physical drivers of extreme water levels

The effect of different forcing agents on the maximum water levels was determined at several stations throughout the estuary (Figure 2a) in a series of numerical experiments (Run 8 to Run 14, Table 3). The surge was computed by subtracting the time series obtained by forcing the model only with the tide and a climatological river flow (Run 8) from those obtained in the standard simulation (Run 1). The maximum value of the surge was then extracted at each station (black bars in Figure 12). At the upstream stations, analyzing the whole time series could mask the effect of the different processes because the maximum water level can be higher on February 16 due to the growth of the river flow (Figure 4). Hence, the analysis was only performed for the second high tide of February 15.

In general, the total surge is amplified as it propagates along the estuary, growing from about 1 m at the inlet mouth (P. Arcos) to 1.3 m at Alcochete. This growth may seem due to resonance, which amplifies semi-diurnal tides by 25% between the same two stations (Fortunato et al., 1999). However, the time scale of the passage of the pressure front is about one day. Since the resonance period of the estuary is about 8 to 9 hours, diurnal signals are not affected by resonance (Fortunato et al., 1997). In order to find an alternative explanation for the surge amplification, the individual contribution of each driving process was analyzed.

The importance of each forcing was determined by switching off the forcing agents individually (Table 3), and again evaluating the surge by subtraction of the results of Run 8. Switching off the forcing agents individually, rather than including them individually, maximizes the reproduction of the non-linear interactions. Results are summarized in Figure 12.

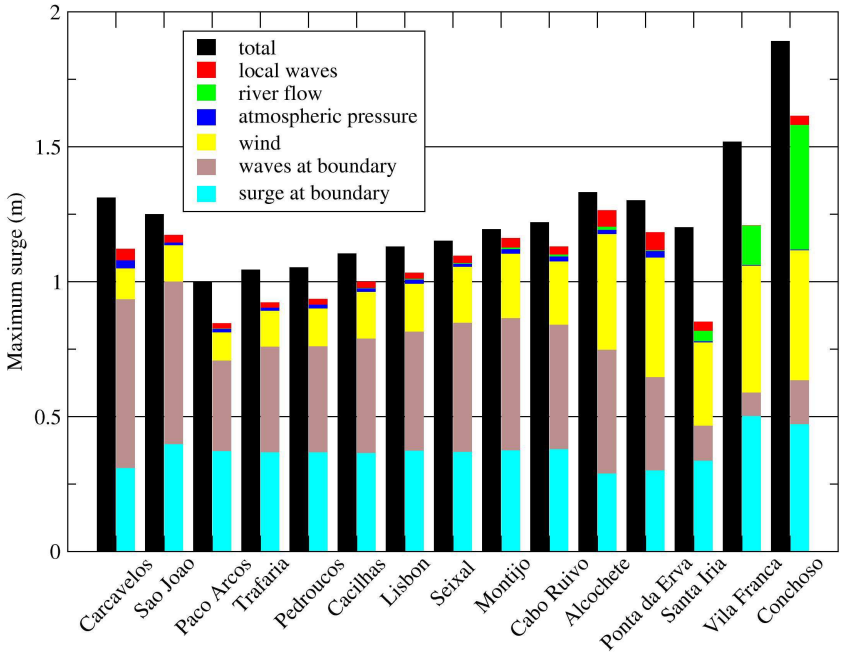

Figure 12. Maximum surge at different stations throughout the estuary.

The impact of the surge at the ocean boundary on the surge in the estuary is fairly constant in space. This behavior is similar to diurnal tidal constituents, whose amplitude is almost constant throughout the estuary. Given the modest amplitude of this component of the surge (30-40 cm in the estuary) compared to the tide, and its long period, the associated velocities and the corresponding frictional losses should be small. The surge is somewhat amplified in the upstream part of the estuary (Vila Franca and Conchoso), probably due to the convergence of the estuary cross-section.

The swell coming in from the ocean boundary has a significant impact on the estuarine water levels, with a maximum wave setup of 33 cm at the inlet mouth (P. Arcos). The development of a substantial wave-induced setup inside estuaries and lagoons during storms, like the one observed herein, has been identified in previous studies, using both models and observations. During storms, radiation stress gradients can be a leading term in the momentum balance in a tidal inlet (Olabarrieta et al., 2011, Wargula et al., 2014). As a result, the effect of wave-induced setup on extreme water levels can reach tens of centimeters inside estuaries and lagoons (Xie et al., 2008; Bertin et al., 2009; Malhadas et al., 2009; Olabarrieta et al., 2011). Bertin et al. (2015) explain this phenomenon by huge onshore-directed wave forces induced by the breaking of storm waves over ebb deltas and rocky shoals. Our results show that these large wave-induced setups can also occur in large estuaries, such as the Tagus.

Furthermore, this maximum wave setup of 33 cm at the inlet mouth grows to about 50 cm in the wide part of the estuary. Yet, a simulation forced only by constant 10 m waves at the ocean boundary (i.e., with the tides switched off and the water elevation fixed at mean sea level) shows a homogeneous wave setup of 20 cm within the estuary. Hence, the growth of the wave setup is attributed to the modulation of the wave setup by the tidal elevations and currents. A similar modulation of the wave setup by tides was proposed by Olabarrieta et al. (2011).

This modulation effectively generates a semi-diurnal pattern in the setup. This hypothesis is confirmed by forcing the model only with tides (M2 and harmonics), a constant wave from the West (significant wave height: 10 m; peak period: 15 s) and a constant river flow (Run 15). Results show that the wave setup grows significantly during ebb and decreases on flood (Figure 13). Two physical processes can contribute to this tidal modulation. First, ebb currents increase the wave height and steepness (Dodet et al., 2013), thereby shifting the position of the breaking point seaward. Secondly, a significant fraction of the highest waves break on the terminal lobe of the ebb delta at low tide, generating strong radiation stress gradients and a high setup. At high tide, this fraction decreases. The waves that do not break over the ebb delta propagate into the inlet or to the coast, and contribute less to the setup inside the estuary. Switching off the effect of tidal currents on wave propagation has a relatively small impact on wave setup (Figure 13a), showing that the latter process clearly dominates. This result is confirmed by running simulations forced by waves alone, but with different mean sea levels. The setup increases to 24 cm when the mean sea level is lowered by 1.5 m, and it decreases to 18 cm when the mean sea level is raised by 1.5 m.

While the varying widths of the surf zone during the tidal cycle elucidate the higher setup at low tide, they do not explain the phase lag observed between the tide and surge signals shown in Figure 13. A possible interpretation is the following. The waves generate very strong currents in the inlet mouth. These currents increase the bottom stress, thus reducing the celerity of the tidal wave. Indeed, the high tides in Run 16 occur about 4-5 minutes later than in Run 15. This phase lag is then at least partially responsible for the phase shift between the surge and the tide in Figure 13.

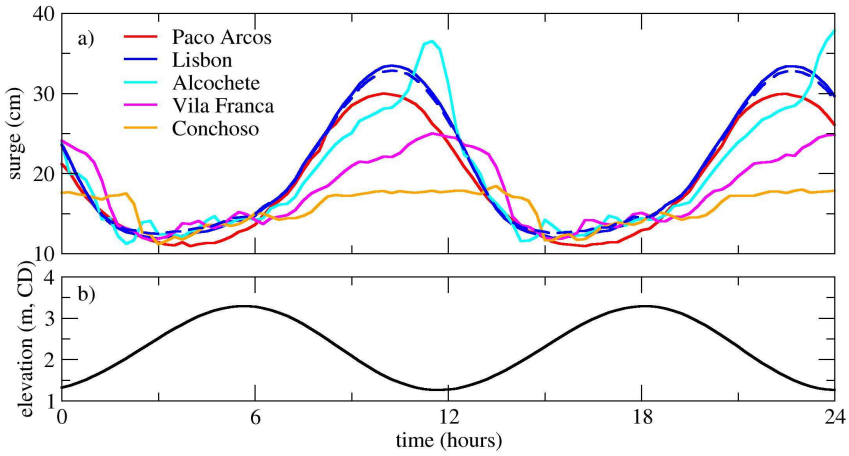

Figure 13. Tide-surge interaction in the Tagus estuary: a) evolution of the wave-induced setup along the estuary; b) tidal elevations at Cascais. The dashed line in a) corresponds to a simulation in which the effect of velocities on wave propagation was switched off.

This tidal modulation is amplified by resonance within the estuary (Figure 13a): the maximum wave setup grows from 30 cm at P. Arcos to 38 cm at Alcochete in Run 15. This behavior of the wave setup contributes therefore to the growth of the surge within the estuary. In the upstream part of the estuary, the impact of the swell declines, although it remains non-negligible (above 10 cm) even upstream of the tidal intrusion limit.

Because the higher setup occurs close to low tide, the impact of the wave setup amplification on the maximum water elevations inside the estuary is small. In contrast, the surge coming from the ocean boundary is independent from the tidal phase and plays therefore a more important role in determining the extent of the inundation.

Wind effects can also be significant. In the wide part of the estuary (Alcochete, Ponta da Erva), they can even be the dominant mechanism for the surge. Not only is the estuary particularly wide (exceeding 10 km near Alcochete), but the fetch can exceed 20 km for some particular wind directions. Furthermore, the wind setup peaks at high tide when the fetch reaches its maximum. The wind setup also propagates upstream and is still significant in the riverine portion of the estuary.

The other forcing agents are generally unimportant. The effect of the river flow decreases downstream. In particular, it is negligible from the wide part of the estuary downstream. This behavior was previously identified by Vargas et al. (2008). Local waves are small, only exceeding 1 m in the deeper channels of the upper estuary. Hence, their effect is modest (up to about 5 cm). Similarly, the effect of atmospheric pressure gradients is negligible at these small scales.

Non-linear effects are seen in Figure 12 as the difference between the total surge and the sum of the individual contributions. These effects are significant and contribute to the surge everywhere inside the estuary. They are particularly important in the riverine part of the domain. Guerreiro et al. (2015) analyzed the effect of sea level rise on the Tagus tidal propagation and concluded that it shifts the resonance period to lower frequencies, thereby increasing the resonance amplification of semi-diurnal tides. The non-linear effects shown in Figure 12 probably have the same origin: each factor increases the mean water level inside the estuary, and thus amplifies the tidal amplitude.

6. SUMMARY AND CONCLUSIONS

A hindcast of the strongest storm that occurred in the 20th century in the Iberian coast was carried out using a suite of atmospheric, oceanic and estuarine models. The models were carefully validated with available data, and the validation was complemented by sensitivity analyses. Overall, the models are shown to provide an accurate simulation of the coastal hydrodynamics, and, in particular, of the water levels and inundation in the Tagus estuary. Since the peak of the atmospheric pressure is overestimated by about 8 hPa, the surge due to the atmospheric pressure alone should be underestimated by at least 8 cm. The ability of the model to reproduce a storm that occurred so many years ago, in 1941, opens interesting perspectives to investigate other old extreme events.

The 1941 storm was one of the most extreme cyclones in terms of impacts on southwestern Europe in the 20th century (Muir-Wood, 2011; Karremann et al., 2016). Its genesis occurred on the subtropical North Atlantic and intensified rapidly on 15 February near 20ºW and 35ºN.The wind storm made landfall during the period of maximum deepening in Portugal, with winds close to 30 m/s in the south of Portugal. The cyclone then crossed the Iberian Peninsula and moved northeast, heading towards the Bay of Biscay and the British Islands.

The cyclone generated waves with a significant wave height close to 14 m to the south of its track. These waves were particularly severe in the Tagus estuary area and further south, where their return period was over 100 years.

In spite of the severity of the storm and the resulting waves, the maximum sea levels only reach the thresholds associated to return periods between 2 and 20 years (increasing northward). These relatively modest return periods are due to the tidal range during which the storm occurred, which corresponds to the percentile 91 of the tidal ranges.

Several physical processes contribute to the extreme water levels in the estuary. The storm surge at the ocean boundary contributes with 30 to 50 cm to the surge in the estuary. The signal propagates almost unchanged along most of the estuary, and is amplified at the bay head, where the estuary narrows. The wave setup associated with the incoming swell is the second most important source of surge in the estuary. This setup is modulated by tides and amplified by resonance through the following processes. At low tide, the highest waves break on the terminal lobe of the ebb delta. The surf zone is narrow, the radiation stress gradients are high and so is the setup. At high tide, a larger fraction of the waves do not break over the ebb delta, but rather propagate to the coast or into the inlet, and their contribution to the wave setup inside the estuary is smaller. This variation of the wave breaking conditions along the tidal cycle thus generates a periodic pattern in the wave setup at the estuary mouth. As the wave setup propagates along the estuary, it is amplified by resonance, much like the tidal wave, because it shares the same period as the tide. Finally, wind effects can also be important in the upper estuary, where the fetch is longest and depths are small. The effect of the river flow is restricted to the narrow, riverine-like part of the estuary.

The models were used to determine the inundation that a major storm would cause today in this estuary. It is shown that there is a submersion hazard of the fertile lands in the upper estuary, in spite of the extensive dikes that surround them. The total area threatened by inundations grows from 25 km^2, if the 1941 event were to happen today, to 77 km^2 if sea level rises by 0.5 m. A present-day worst case scenario, obtained by combining the 1941 storm with an extreme tidal range, would flood over 40 km^2 of agricultural land. These results will support risk analyses and the definition of adaptation measures to cope with future extreme events.

ACKNOWLEDGEMENTS

ABF, PF and MR were partially funded by the European Commission through the H2020 project BINGO (Grant Agreement Number 641739). MR was also partially funded by a post-doctoral grant from FCT – Fundação para a Ciência e a Tecnologia (SFRH/BPD/87512/2012). XB received funding from the European Commission through the FP7 project Risc-Kit (Grant Agreement Number 603458). JF and MLRL were partially supported by FEDER funds through the COMPETE (Programa Operacional Factores de Competitividade) programme and by national funds through the FCT project STORMEx FCOMP-01-0124-FEDER-019524 (PTDC/AAC-CLI/121339/2010). This work took advantage of the Portuguese National Distributed Computing Infrastructure (INCD). The authors would like to thank Drs. Elsa Alves and Rui Rodrigues for useful discussions about the river flow. The constructive comments of Diogo Mendes and two anonymous reviewers are also acknowledged. The authors thank the various institutions that provided data, models and model results mentioned in the text.

REFERENCES

Almeida, L.P., Ferreira, O., Vousdoukas, M.I., Dodet, G., 2011. Historical variation and trends in storminess along the Portuguese South Coast, *Natural Hazards and Earth System Sciences*, 11/9: 2407-2417. DOI:10.5194/nhess-11-2407-*2011*.

Antunes, C., Taborda, R., 2009. Sea level at Cascais tide gauge: data, analysis and results. *Journal of Coastal Research*, Special Issue 56: 218 – 222.

Azevedo, A., Oliveira, A., Fortunato, A.B., Zhang, J., Baptista, A.M., 2014. A cross-scale numerical modeling system for management support of oil spill accidents, *Marine Pollution Bulletin* 80, 1-2: 132 – 147. DOI: 10.1016/j.marpolbul.2014.01.028

Bertin, X., Fortunato, A.B., Oliveira, A., 2009. A modeling-based analysis of processes driving wave-dominated inlets, Continental Shelf Research, 29/5–6: 819–834, DOI: 10.1016/j.csr.2008.12.019.

Bertin, X., Bruneau, N., Breilh, J.-F., Fortunato, A.B., Karpytchev, M., 2012. Importance of wave age and resonance in storm surges: The case Xynthia, Bay of Biscay. *Ocean Modelling* 42/1: 16-30. DOI: 10.1016/j.ocemod.2011.11.001

Bertin, X., Prouteau, E., Letetrel, C., 2013. A significant increase in wave height in the North Atlantic Ocean over the 20th century, *Global and Planetary Change*, 106: 77-83. DOI:10.1016/j.gloplacha.2013.03.009.

Bertin, X., Li, K., Roland, A., Zhang, Y.J., Breilh, J.-F., Chaumillon, E., 2014. A modeling-based analysis of the flooding associated with Xynthia, central Bay of Biscay, *Coastal Engineering*, 94: 80-89. DOI: 10.1016/j.coastaleng.2014.08.013

Bertin, X., Li, K., Roland, A., Bidlot, J.R., 2015. The contribution of short waves in storm surges: two recent examples in the central part of the Bay of Biscay, *Continental Shelf Research*, 96: 1-15. DOI: 10.1016/j.csr.2015.01.005

Bidlot, J.R., Janssen, P.A.E.M., Abdalla, S., 2007. A revised formulation for ocean wave dissipation and its model impact, *Tech. Memo*, **509**, 29

Bilskie, M.V., Coggin, D., Hagen, S.C., Medeiros, S.C., 2015. Terrain-driven unstructured mesh development through semi-automatic vertical feature extraction, *Advances in Water Resources*, 86/A: 102-118. DOI: 10.1016/j.advwatres.2015.09.020

Bilskie, M.V., Hagen, S.C., Medeiros, S.C., Cox, A.T., Salisbury, M., Coggin, D., 2016. Data and numerical analysis of astronomic tides, wind-waves, and hurricane storm surge along the northern Gulf of Mexico, *Journal of Geophysical Research: Oceans*, 121, DOI: 10.1002/2015JC011400.

Bouws, E., Komen, G.J., 1983. On the balance between growth and dissipation in an extreme, depth-limited wind-sea in the southern North Sea. *Journal of Physical Oceanography*, 13, 1653-1658.

Breilh, J.-F., 2014. *Les surcotes et les submersions marines dans la partie centrale du Golfe de Gascogne : les enseignements de la tempête Xynthia*, Ph.D. Thesis, Université de la Rochelle, 225 pp.

Breilh, J.-F., Bertin, X., Chaumillon, E., Giloy, N., Sauzeau, T., 2014. How frequent is storm-induced flooding in the central part of the Bay of Biscay? *Global and Planetary Change*, 122: 161-175. DOI: 10.1016/j.gloplacha.2014.08.013

Canas, A., Santos, A., Leitão, P. (2009). Effect of large-scale atmospheric pressure changes on water level in the Tagus estuary, *Journal of Coastal Research*, Special Issue 56, 1627-1631.

Carrère, L., Lyard, F., Cancet, M., Guillot, A., Roblou, L., 2012. FES2012: A new global tidal model taking taking advantage of nearly 20 years of altimetry, *Proceedings of meeting "20 Years of Altimetry"*.

Chen, F., Dudhia, J., 2001. Coupling an advanced land surface–hydrology model with the Penn State–NCAR MM5 modeling system. Part I: model implementation and sensitivity. *Monthly Weather Review*, 129: 569–585. DOI: 10.1175/1520-0493(2001)129<0569:CAALSH>2.0.CO;2

Chen, J., Chen, J., Liao, A., Cao, X., Chen, L., Chen, X., He, C., Peng, S., Lu, M., Zhang, W., Tong, X., Mills, J., 2015. Global land cover mapping at 30 m resolution: A POK-based operational approach, *ISPRS Journal of Photogrammetry and Remote Sensing*: DOI: 10.1016/j.isprsjprs.2014.09.002.

Companhia das Lezírias, 1941. Relatório do exercício de 1940, presente à assembleia-geral de accionistas de 1 de Abril de 1941. Lisboa, 1941. AHCL. Torre do Tombo (in Portuguese).

Compo, G.P., Whitaker, J.S., Sardeshmukh, P.D., Matsui, N., Allan, R.J., Yin, X., Gleason, B.E., Vose, R.S., Rutledge, G., Bessemoulin, P., Brönnimann, S., Brunet, M., Crouthamel, R.I., Grant, A.N., Groisman, P.Y., Jones, P.D., Kruk, M.C., Kruger, A.C., Marshall, G.J., Maugeri, M., Mok, H.Y., Nordli, Ø., Ross, T.F., Trigo, R.M., Wang, X.L., Woodruff, S.D., Worley, S.J., 2011. The twentieth century reanalysis project, *Quarterly Journal of the Royal Meteorological Society*, 137: 1–28. DOI:10.1002/qj.77

Dee, D.P., Uppala, S.M., Simmons, A.J., Berrisford, P., Poli, P., Kobayashi, S., Andrae, U., Balmaseda, M.A., Balsamo, G., Bauer, P., Bechtold, P., Beljaars, A.C.M., van de Berg, L., Bidlot, J., Bormann, N., Delsol, C., Dragani, R., Fuentes, M., Geer, A.J., Haimberger, L., Healy, S.B., Hersbach, H., Hólm, E.V., Isaksen, L., Kållberg, P., Köhler, M., Matricardi, M., McNally, A.P., Monge-Sanz, B.M., Morcrette, J.-J., Park, B.-K., Peubey, C., de Rosnay, P., Tavolato, C., Thépaut, J.-N., Vitart, F., 2011. The ERA-Interim reanalysis: configuration and performance of the data assimilation system. *Quarterly Journal of the Royal Meteorological Society,* 137, 553–597. DOI: 10.1002/qj.828.

Dietrich, J.C., Bunya, S., Westerink, J.J., Ebersole, B.A., Smith, J.M., Atkinson, J.H., Jensen, R., Resio, D.T., Luettich, R.A., Dawson, C., Cardone, V.J., Cox, A.T., Powell, M.D., Westerink, H.J., Roberts, H.J., 2010. A High-Resolution Coupled Riverine Flow, Tide, Wind, Wind Wave and Storm Surge Model for Southern Louisiana and Mississippi: Part II – Synoptic Description and Analysis of Hurricanes Katrina and Rita. *Monthly Weather Review*, 138: 378-404. DOI: 10.1175/2009MWR2907.1

Dodet, G., Bertin, X., Bruneau, N., Fortunato, A.B., Nahon, A., Roland, A., 2013. Wave-current interactions in a wave-dominated tidal inlet, *Journal of Geophysical Research: Oceans* 118, 3: 1587 - 1605. DOI: 10.1002/jgrc.20146.

Dudhia, J., 1989. Numerical study of convection observed during the winter monsoon experiment using a mesoscale two-dimensional model. *J. Atmos. Sci.*, 46, 3077-3107. DOI: 10.1175/1520-0469(1989)046<3077:NSOCOD>2.0.CO;2

Ferreira, J.A., Carvalho, A.C., Carvalheiro, L., Rocha, A., Castanheira, J.M. 2014. On the influence of physical parameterizations and domains configuration in the simulation of an extreme precipitation event. *Dynamics of Atmospheres and Oceans*, 68: 35-55, ISSN 0377-0265. doi: 10.1016/j.dynatmoce.2014.08.001

Ferreira J.A., Liberato M.L.R., Ramos A.M., 2016. On the relationship between atmospheric water vapour transport and extra-tropical cyclones development. *Physics and Chemistry of the Earth*, Parts A/B/C doi: 10.1016/j.pce.2016.01.001

Fortunato, A.B., Baptista, A.M., Luettich, Jr., R.A., 1997. A three-dimensional model of tidal currents in the mouth of the Tagus Estuary, *Continental Shelf Research*, 17/14: 1689-1714. DOI: 10.1016/S0278-4343(97)00047-2

Fortunato, A.B., Oliveira, A., Baptista, A.M., 1999. On the effect of tidal flats on the hydrodynamics of the Tagus estuary. *Oceanologica Acta*, 22/1: 31-44. DOI:10.1016/s0399-1784(99)80030-9.

Fortunato, A.B., Bruneau, N., Azevedo, A., Araújo, M.A.V.C., Oliveira, A., 2011. Automatic improvement of unstructured grids for coastal simulations, *Journal of Coastal Research*, Special Issue I64: 1028-1032.

Fortunato, A.B., Rodrigues, M., Dias, J.M., Lopes, C., Oliveira, A., 2013. Generating inundation maps for a coastal lagoon: a case study in the Ria de Aveiro (Portugal), *Ocean Engineering*, 64: 60-71. DOI: 10.1016/j.oceaneng.2013.02.020

Fortunato, A.B., Li, K., Bertin, X., Rodrigues, M., Miguez, B.M., 2016. Determination of extreme sea levels along the Iberian Atlantic coast, *Ocean Engineering*, 111/1: 471-482. DOI: 10.1016/j.oceaneng.2015.11.031

Fortunato, A.B., Oliveira, A., Rogeiro, J., Tavares da Costa, R., Gomes, J.L., Li, K., Jesus, G., Freire, P., Rilo, A., Mendes, A., Rodrigues, M., Azevedo, A. (2017). Operational forecast framework applied to extreme sea levels at regional and local scales, *Journal of Operational Oceanography*. DOI: 10.1080/1755876X.2016.1255471

Freitas, J.G., Dias J.A., 2013. 1941 windstorm effects on the Portuguese Coast. What lessons for the future? *Journal of Coastal Research*, Special Issue 65: 714-719. DOI : 10.2112/SI65-121.

Freire, P., Taborda, R. Silva, A., 2007. Sedimentary characterization of Tagus estuarine beaches (Portugal). A contribution to the sediment budget assessment. *Journal of Soils and Sediment*s, 7/5: 296-302. DOI:10.1065/jss2007.08.243.

Freire, P., Ferreira, Ó., Taborda, R., Oliveira, F.S.B.F., Carrasco, A.R., Silva, A., Vargas, C., Capitão, R., Fortes, C.J., Coli, A.B., Santos, J.A., 2009. Morphodynamics of fetch-limited beaches in contrasting environments, *Journal of Coastal Research*, Special Issue 56, 183-187.

Freire, P., Tavares, A., Sá, L., Oliveira, A., Fortunato, A.B., Santos, P.P., Rilo, A., Gomes, J.L., Rogeiro, J., Pablo, R., Pinto, P.J., 2016. A local scale approach to estuarine flood risk management, *Natural Hazards*, doi:10.1007/s11069-016-2510-y

Ganho, N., 2013. Risco de ventos tempestuosos de escala sinóptica em Portugal continental: análise causal, in *Riscos naturais, antrópicos e mistos. Homenagem ao Professor Doutor Fernando Rebelo*, Universidade de Coimbra, pp. 251-266 (in Portuguese).

Grell, G.A., Devenyi, D., 2002. A generalized approach to parameterizing convection combining ensemble and data assimilation techniques. *Geophysical Research Letters*, 29 (14). DOI: 10.1029/2002GL015311

Guérin, T., Bertin, X., Dodet, G., 2016. A numerical scheme for coastal morphodynamic modelling on unstructured grids, *Ocean Modelling*, 104, 45-53. DOI: 10.1016/j.ocemod.2016.04.009

Guerreiro, M., Fortunato, A.B., Freire, P., Rilo, A., Taborda, R., Freitas, M.C., Andrade, C., Silva, T., Rodrigues, M., Bertin, X., Azevedo, A. (2015). Evolution of the hydrodynamics of the Tagus estuary (Portugal) in the 21st century. *Revista de Gestão Costeira Integrada*, 15/1: 65-80. DOI: 10.5894/rgci515

Hasselmann, K., Barnett, T.P., Bouws, E., Carlson, H., Cartwright, D.E., Enke, K., Ewing, J.A., Gienapp, H., Hasselmann, D.E., Kruseman, P., Meerburg, A., Muller, P., Olbers, D.J., Richter, K., Sell., W., Walden, H., 1973. *Measurements of wind-wave growth and swell decay during the Joint North Sea Wave Project (JONSWAP)*, Dtsch. Hydrogr. Z. Suppl., 12, A8, 1-95.

Hong, S.-Y., Lim, J.-O.J., 2006. The WRF Single-Moment 6-Class Microphysics Scheme (WSM6). *Journal of the Korean Meteorological Society*, 42: 129-151.

IPCC, 2013. Climate change 2013: the physical science basis. Contribution of Working Group I to the fifth assessment report of the Intergovernmental Panel on Climate Change. Cambridge University Press, Cambridge, U.K. and New York, N.Y., USA, 1132 pp.

Karremann, M.K., Liberato, M.L.R., Ordóñez, P., Pinto, J.G., 2016 Characterization of synoptic conditions and cyclones associated with top ranking potential wind loss events over Iberia. *Atmospheric Science Letters*, 17: 354–361. DOI: 10.1002/asl.665

Goutx, D., Baraer, F., Roche, A., Jan, G., 2014. Ces tempêtes extrêmes que l'histoire ne nous a pas encore dévoilées. *La houille Blanche*, 2, 27-33 (in French). DOI 10.1051/lhb/2014013.

Le Roy, S., Pedreros, R., Andre, C., Paris, F., Lecacheux, S., Marche, F., Vinchon, C., 2015. Coastal flooding of urban areas by overtopping: dynamic modelling application to the Johanna storm (2008) in Gavres (France), *Natural Hazards and Earth System Sciences*, 15/11: 2497-2510. DOI: 10.5194/nhess-15-2497-2015

Liberato, M.L.R., Pinto, J.G., Trigo, R.M., Ludwig, P., Ordõnez, P., Yuen, D., Trigo, I.F., 2013. Explosive development of winter storm Xynthia over the subtropical North Atlantic Ocean. *Natural Hazards and Earth System Science*, 13, 2239–2251. DOI: 10.5194/nhess-13-2239-2013.

Lin, N., Emanuel, K., 2016. Grey swan tropical cyclones. *Nature Climate Change*, 6: 106–111. DOI: 10.1038/NCLIMATE2777

Lopes, C.L.B., 2016. Flood risk assessment in Ria de Aveiro under present and future scenarios, Ph.D. thesis, University of Aveiro, 224pp (in Portuguese).

Lopes, C.L., Silva, P.A., Dias, J.M., Rocha, A., Picado, A., Plecha, S., Fortunato, A.B., 2011. Local sea level change scenarios for the end of the 21st century and potential physical impacts in the lower Ria de Aveiro (Portugal), *Continental Shelf Research* 31, 14: 1515 - 1526. DOI: 10.1016/j.csr.2011.06.015

Lowe, J.A., Gregory, J.M., 2005. The effects of climate change on storm surges around the United Kingdom, *Philosophical Transactions of the Royal Society A*, 363: 1313–1328. DOI: 10.1098/rsta.2005.1570.

Madaleno, I.M., 2006. Companhia das Lezírias – o passado e o presente. Hispania Nova. Revista de História Contemporânea, 6, http://hispanianova.rediris.es. (in Portuguese).

Malhadas, M.S., Leitão, P.C., Silva, A., Neves, R., 2009. Effect of coastal waves on sea level in Óbidos Lagoon, Portugal, *Continental Shelf Research*, 19/9: 1240–1250, DOI: 10.1016/j.csr.2009.02.007.

Marcos, M., Jorda, G., Gomis, D., Perez, B., 2011. Changes in storm surges in southern Europe from a regional model under climate change scenarios, *Global and Planetary Change*, 77/3-4: 116-128. DOI: 10.1016/j.gloplacha.2011.04.002

Melet, A., Almar, R., Meyssignac, B., 2016. What dominates sea level at the coast: a case study for the Gulf of Guinea, *Ocean Dynamics*, 66/5: 623–636. DOI 10.1007/s10236-016-0942-2

Mlawer, E.J., Taubman, S.J., Brown, P.D., Iacono, M.J., Clough, S.A., 1997. Radiative transfer for inhomogeneous atmosphere: RRTM, a validated correlated-k model for the long-wave. *Journal of Geophysical Research*, 102 (D14), 16663-16682.

Muir-Wood, R., 2011. The 1941 February 15th Windstorm in the Iberian Peninsula. *Trébol*, 56: 4-13.

Neves, F.S., 2010. *Dynamics and hydrology of the Tagus estuary: results from in situ observations*. 210p, Ph.D. thesis, Universidade de Lisboa, Portugal. Unpublished. Available at: http://repositorio.ul.pt/handle/10451/2003

Noh, Y., Cheon, W.G., Hong, S.-Y., Raasch, S., 2003. Improvement of the K-profile model for the planetary boundary layer based on large eddy simulation data. *Bound-Layer Meteorology*, 107, 401-427.

Nunes, A., Pinho, J., Ganho, N., 2012. O Ciclone de Fevereiro de 1941: análise histórico-geográfica dos seus efeitos no município de Coimbra, *Cadernos de Geografia*, 30/31: 53-60 (in Portuguese).

Olabarrieta, M., Warner, J. C., Kumar, N., 2011. Wave-current interaction in Willapa Bay, *Journal of Geophysical Research*, 116, C12014, DOI: 10.1029/2011JC007387.

Oliveira, F.S.B.F., 2000. Numerical simulation of wave propagation in the entrance of the Tagus estuary, M.L. Spaulding, H.L. Butler (Eds.), Proceedings of the Sixth Conference on Estuarine and Coastal Modeling, ASCE, pp. 510–525.

Perini, L., Calabrese, L., Salerno, G., Ciavola, P., Armaroli, C., 2016. Evaluation of coastal vulnerability to flooding: comparison of two different methodologies adopted by the Emilia-

Romagna region (Italy), *Natural Hazards and Earth System Science*, 16: 181-194. DOI: 10.5194/nhess-16-181-2016.

Pinto, L., Fortunato, A.B., Zhang, Y., Oliveira, A., Sancho, F.E.P., 2012. Development and validation of a three-dimensional morphodynamic modelling system for non-cohesive sediments, *Ocean Modelling*, 57-58: 1-14. DOI: 10.1016/j.ocemod.2012.08.005

Rilo, A., Freire, P., Ceia, R., Mendes, R.N., Catalão, J., Taborda, R., 2012. Human effects on estuarine shoreline decadal evolution. *Geophysical Research Abstracts*, Vol. 14, EGU2012-10863, 2012, EGU General Assembly 2012.

Rilo, A., Freire, P., Mendes, R.N., Ceia, R., Catalão, J., Taborda, R., Melo, R., Caçador, M.I., Freitas, M.C., Fortunato, A.B., Alves, E., 2014. Methodological framework for the definition and demarcation of the highest astronomical tide line in estuaries: the case of Tagus Estuary (Portugal), *Revista de Gestão Costeira Integrada*, 14/1: 95-107 (in Portuguese). DOI: 10.5894/rgci450.

Rodrigues, M., Oliveira, A., Queiroga, H., Fortunato, A.B., Zhang, Y.J., 2009. Three-dimensional modeling of the lower trophic levels in the Ria de Aveiro (Portugal), *Ecological Modelling* 220, 9-10: 1274 – 1290. DOI: 10.1016/j.ecolmodel.2009.02.002

Rodrigues, M., Oliveira, A., Guerreiro, M., Fortunato, A.B; Menaia, J., David, L.M.; Cravo, A. 2011. Modeling fecal contamination in the Aljezur coastal stream (Portugal), *Ocean Dynamics* 61/6: 841-856. DOI: 10.1007/s10236-011-0392-9

Rodrigues, M., Fortunato, A.B., Freire, P., 2016. Salinity evolution in the Tagus estuary relative to climate change, *Actas das 4as Jornadas de Engenharia Hidrográfica, Instituto Hidrográfico*, Lisbon, 179-182.

Roland, A., Zhang, Y.J., Wang, H.V., Meng, Y., Teng, Y.-C., Maderich, V., Brovchenko, I., Dutour-Sikiric, M., Zanke, U. (2012). A fully coupled 3D wave-current interaction model on unstructured grids. *Journal of Geophysical Research*, 117, C00J33. DOI: 10.1029/2012JC007952.

Rusu, L., Bernardino, M., Guedes Soares, C., 2009. Influence of wind resolution on the prediction of waves generated in an estuary, *Journal of Coastal Research*, Special Issue 56: 1419-1423.

Rusu, L., Bernardino, M., Guedes Soares, C., 2011. Modelling the influence of currents on wave propagation at the entrance of the Tagus estuary, *Ocean Engineering*, 38: 1174-1183. DOI: 10.1016/j.oceaneng.2011.05.016

Salgueiro, A.R., Machado, M.J., Barriendos, M., Pereira, H.G., Benito, G., 2013. Flood magnitudes in the Tagus River (Iberian Peninsula) and its stochastic relationship with daily North Atlantic Oscillation since mid-19th Century, *Journal of Hydrology*, 502: 191–201. DOI: 10.1016/j.jhydrol.2013.08.008

Skamarok, W.C., Klemp, J.B., Dudhia, J., Gill, D.O., Barker, D.M., Duda, M.G., Huang, X.Y., Wang, W., Powers, J.G., 2008. *A description of the advanced research WRF Version 3*. NCAR Technical Note.

Schloen, J., Stanev, E.V., Grashorn, S., 2017. Wave-current interactions in the southern North Sea: The impact on salinity, *Ocean Modelling*, 111: 19–37. DOI: 10.1016/j.ocemod.2017.01.003

Stucki, P., Brönnimann, S., Martius, O, Welker, C., Rickli, R., Dierer, S., Bresch, D.N., Compo, G.P., Sardeshmukh, P.D., 2015. Dynamical downscaling and loss modeling for the reconstruction of historical weather extremes and their impacts: a severe Foehn storm in 1925. *Bulletin of the American Meteorological Society*. 96: 1233–1241. DOI: http://dx.doi.org/10.1175/BAMS-D-14-00041.1

Tavares, A.O., Santos, P.P., Freire, P., Fortunato, A.B., Rilo, A., Sá, L., 2015. Flooding hazard in the Tagus estuarine area: the challenge of scale in vulnerability assessments. *Environmental Science & Policy*, 51: 238-255. DOI: 10.1016/j.envsci.2015.04.010.

Tolman, H.L., 2009. User manual and system documentation of WAVEWATCH III, version 3.14. NOAA/NWS/NCEP/MMAB Technical Note 276, 194 p.

Tomás, A., Méndez, F.J., Medina, R., Jaime, F.F., Higuera, P., Lara, J.L., Ortiz, M.D., Álvarez de Eulate, M.F., 2015. A methodology to estimate wave-induced coastal flooding hazard maps in Spain, *Journal of Flood Risk Management*, DOI: 10.1111/jfr3.12198.

Turner, P., Baptista, A.M., 1993. ACE/gredit User's Manual. Software for Semi-automatic Generation of Two-Dimensional Finite Element Grids. Center for Coastal and Land-Margin Research, Oregon Graduate Institute of Science & Technology.

Ulbrich, U., Leckebusch, G.C., Grieger, J., Schuster, M., Akperov, M., Bardin, M.Y., Feng, Y., Gulev, S., Inatsu, M., Keay, K., Kew, S.F., Liberato, M.L.R., Lionello, P., Mokhov, I.I., Neu, U., Pinto, J.G., Raible, C.C., Reale, M., Rudeva, I., Simmonds, I., Tilinina, N.D., Trigo, I.F., Ulbrich, S., Wang, X.L., Wernli, H., and The IMILAST team, 2013. Are greenhouse gas signals of northern hemisphere winter extra-tropical cyclone activity dependent on the identification and tracking algorithm? *Meteorologische Zeitschrift*, 22/1: 61-68. DOI: 10.1127/0941-2948/2013/0420.

Vargas, C., Oliveira, F.S.B.F., Oliveira, A., Charneca, N., 2008. Flood vulnerability analysis of an estuarine beach: application to Alfeite sand spit (Tagus Estuary). *Revista de Gestão Costeira Integrada / Integrated Coastal Zone Management Journal*, 8/1: 25-43. DOI: 10.5894/rgci26

Vousdoukas, M.I., Voukouvalas, E., Annunziato, A., Giardino, A., Feyen, L., 2016. Projections of extreme storm surge levels along Europe, *Climate Dynamics*, DOI: 10.1007/s00382-016-3019-5.

Xie, L., Liu, H., Peng, M., 2008. The effect of wave–current interactions on the storm surge and inundation in Charleston Harbor during Hurricane Hugo 1989, *Ocean Modelling*, 20/3: 252-269, DOI: http://dx.doi.org/10.1016/j.ocemod.2007.10.001.

Wargula, A., Raubenheimer, B., Elgar, S., 2014, Wave-driven along-channel subtidal flows in a well-mixed ocean inlet, *Journal of Geophysical Research*: Oceans, 19: 2987–3001, DOI: 10.1002/2014JC009839.

Zampato, L., Bajo, M., Canestrelli, P., Umgiesser, G. (2016). Storm surge modelling in Venice: two years of operational results, *Journal of Operational Oceanography*, 9: S46-S57. DOI: 10.1080/1755876X.2015.1118804

Zhang, Y., Baptista, A.M., 2008. SELFE: A semi-implicit Eulerian-Lagrangian finite-element model for cross-scale ocean circulation. *Ocean Modeling*, 21(3-4), 71-96. DOI: 10.1016/j.ocemod.2007.11.005.

Zhang, Y.J., Ye, F., Stanev, E.V., Grashorn, S., 2016. Seamless cross-scale modeling with SCHISM, *Ocean Modelling*, 102: 64-81. DOI:10.1016/J.OCEMOD.2016.05.002.

Zorndt, A., Goseberg, N., Schlurmann, T., 2014. Influence of retention areas on the propagation of storm surges in the Weser estuary. *Coastal Engineering Proceedings, 1*(34), management.51. DOI: 10.9753/icce.v34.management.51